539.107.6

METHODS OF HIGH-ENERGY PARTICLE SEPARATION

V. A. VAGIN, V. I. KOTOV, and I. N. SEMENYUSHKIN

Usp. Fiz. Nauk 82, 707-748 (April, 1964)

I. Introduction . . . 305
II. Separation by Using the Distinguishing Features of the Interaction Between Particles and Their Decay Properties . . . 305
III. Electrostatic Separators . . . 309
IV. Electrodynamic Separators . . . 315
Conclusion . . . 327
Literature . . . 327

1. INTRODUCTION

THE rapid development of accelerator technology has added much to the scientists' knowledge of the atomic nucleus. One of the most interesting results of this research is the discovery of a large number of new elementary particles. Naturally, with such an abundance of elementary particles (there are now 30 of them, and apparently this list will be supplemented with new particles) the very concept of "elementary" particle becomes meaningless. What is the raw material of which matter is built? This and many other important questions can be answered only by a systematic investigation of the whole gamut of the particles and their interaction with matter. Experiments of this type entail as a rule great technical difficulties, because most elementary particles are unstable and decay rapidly. On the other hand, the yields of secondary particles of interest to physicists are low and are furthermore accompanied by a strong pion background.

Under such conditions it becomes practically impossible to use devices which are not controlled in time or are not specially adapted for this purpose. These include first various types of bubble chambers, thick emulsions, etc. At the same time, the electronic methods such as scintillation or Cerenkov counters and spark chambers cannot provide exhaustive information on the character of the interaction between the rare particles and matter. To broaden the experimental base it is necessary both to improve further the electronic apparatus and to separate the rare particles. The latter is a very difficult problem, particularly when it comes to the separation of high-energy particles.

Let us consider the relative yields of secondary particles from a bevatron (proton energy 6.3 GeV) and from a proton synchrotron (proton energy 30 GeV), shown in Tables I and II [1,2]. As can be seen from the tables, the particles of greatest interest to contemporary research are K mesons and antiprotons, the yields of which are among the lowest of all secondary-particle yields. The values of η, depending on the energy of the accelerated protons, the momentum of the secondary particles, and other factors, range from 10^{-2} to 10^{-5}. Yet effective operation of, say, a bubble chamber requires that the total number of particles registered during each working cycle must not exceed several dozen (20—40). The number of background particles, naturally, should be at least of the same order of magnitude as the number of the required particles, and the separation coefficient* is by the same token equal to 10^2—10^5.

The main characteristics of the particles are the mass, the electric charge, the spin, magnetic moment, lifetime, etc. In principle a mixture of particles of two or more species can be separated on the basis of differences in any of the foregoing characteristics. However, from the point of view of experimental realization of this problem, i.e., from the point of view of the level of present day technology, preference should be given to such characteristics as mass, charge, and lifetime. The use of electric and magnetic fields and the presence of interaction between charged particles and the medium has made it possible to realize a large number of separation methods. Foremost among them are the absorber method, the method of electrostatic and electrodynamic separation of particles, and a few others.

In the present paper we systematize and describe the existing and proposed methods for the separation of high-energy particles.

II. SEPARATION BY USING THE DISTINGUISHING FEATURES OF THE INTERACTION BETWEEN PARTICLES AND THEIR DECAY PROPERTIES

1. Absorber Method

One of the simplest and oldest methods of separa-

*The separation coefficient is the ratio of the number of background particles to the required particles before and after separation.

Table I. Yields of particles from a bevatron at an accelerated-proton energy 6.3 GeV

Particle	p, MeV/c	Target: Material	Target: Length, cm	Ratio η of the number of "particles" to the number of pions in the target	Remark
K^-	450	Cu	7.5—1·25	1/1000	In all cases the secondary particles leave the target at an angle $\theta = 0°$. The yield of antiprotons ($\tilde{p}$) relative to the pions in the 1 – 3 GeV/c interval amounts to $10^{-5} - 3 \times 10^{-6}$. The maximum value is $\sim 6 \times 10^{-5}$ for $\tilde{p} \simeq 2$ GeV/c.
K^-	1120	Polyethylene		1/140	
K^-	1700	Be	15	1/50	
K^-	2000	Be	15	1/70	
K^-	2800	Be	15	1/70	
K^+	505	Cu	7.5—1·25	1/71	
$\tilde{p}$	450	Be	15	$1/20 \cdot 10^5$	
$\tilde{p}$	600	Be	15	$1/6 \cdot 7 \cdot 10^5$	
$\tilde{p}$	700	Be	15	$1/4 \cdot 2 \cdot 10^5$	
$\tilde{p}$	800	Be	15	$1/2 \cdot 3 \cdot 10^5$	
$\tilde{p}$	1700	Be	15	$1/0 \cdot 22 \cdot 10^5$	
$\tilde{p}$	2000	Be	15	$1/0 \cdot 21 \cdot 10^5$	
$\tilde{p}$	2800	Be	15	$1/0 \cdot 35 \cdot 10^5$	
p	1690	C	5	$1/0 \cdot 25 \cdot 10^5$	

Table II. Yields of particles from a proton synchrotron at an accelerated-proton energy 30 GeV

Particle	p, GeV/c	Target	Ratio η of no. of "particles" to no. of pions in target	Particle	p, GeV/c	Target	Ratio η of no. of "particles" to no. of pions in target	Particle	p, GeV/c	Target	Ratio η of no. of "particles" to no. of pions in target
K^+	4.0	Be	$9 \cdot 10^{-2}$	K^+	9.4	Be	$13 \cdot 10^{-2}$	$\tilde{p}$	6.4	Al	$1 \cdot 10^{-2}$
K^+	5.4	Be	$12 \cdot 10^{-2}$	K^-	5.4	Al	$3 \cdot 10^{-2}$	$\tilde{p}$	7.4	Al	$1 \cdot 10^{-2}$
K^+	6.4	Be	$12 \cdot 10^{-2}$	K^-	6.4	Al	$6 \cdot 10^{-2}$	$\tilde{p}$	8.8	Al	$9 \cdot 10^{-3}$
K^+	7.4	Be	$13 \cdot 10^{-2}$	K^-	7.4	Al	$6 \cdot 10^{-2}$	$\tilde{p}$	11.4	Al	$8 \cdot 10^{-3}$
K^+	11.4	Be	$13 \cdot 10^{-2}$	K^-	8.8	Al	$5 \cdot 10^{-2}$	$\tilde{p}$	12.4	Al	$6 \cdot 10^{-3}$
K^+	13.6	Be	$15 \cdot 10^{-2}$	K^-	11.4	Al	$5 \cdot 10^{-2}$	$\tilde{p}$	14.4	Al	$4 \cdot 10^{-3}$
K^+	15.2	Be	$14 \cdot 10^{-2}$	K^-	16.4	Al	$2 \cdot 10^{-2}$	$\tilde{p}$	16.4	Al	$2 \cdot 10^{-3}$

Remark. In all cases the secondary particles are emitted from the target at an angle $\theta = 4.75°$.

tion of charged particles by their masses is the "absorber method." It is based on the fact that the ionization losses of particles passing through some medium are determined by their velocity.

Assume that we have a single-momentum beam consisting, for example, of two species of particles with different masses. In accordance with the mass difference, the velocity of the particles of one species will differ from that of the other. Consequently, the velocity difference will cause the particles passing through the absorber to be separable by momentum, too. Subsequent magnetic analysis will result in spatial separation of these particles.

As is well known, the expression for the most probable energy (ionization) loss of a particle passing through a layer of matter l g/cm^2 thick, with allowance for the statistical character of the losses, can be represented in the form [3]

$$E_l - E_p = \frac{0.3 Z m_e c^2 l}{\beta^2}\left[\ln \frac{0.6 Z m_e c^2 l}{A(1-\beta^2) I^2(Z)} - \beta^2 + j\right], \quad (2.1)$$

where E_i and E_p are the respective particle energies before and after passing through the matter, Z is the atomic number of the matter and A is its mass number, β is the velocity of the particle in units of the velocity of light c, $m_e c^2$ is the rest mass of the electron, I(Z) is the average ionization potential of an atom with atomic number Z, and j is some function* that depends on the velocity of the particle and on the characteristics of the medium.

However, expression (2.1) does not take into account an important circumstance which must be kept in mind, namely the screening of the electric field of the passing particle by the atoms of the medium—the so-called effect of density of matter. The screening attenuates the interaction and leads to a decrease in the energy loss. This effect increases with increasing particle velocity.

The change in particle momentum after passage through the absorber is

$$d(pc) = \int_0^l \frac{1}{\beta}\left(\frac{dE}{dx}\right) dx. \quad (2.2)$$

*The derivation of the function j is described, for example, in [4]; see also [3].

The maximum beam separation effect is obtained by suitable choice of the decelerating medium. It is desirable to have large ionization losses (small I(Z) and also a small effect of the density of the material). At the same time, the scattering of the particles and their nuclear interaction with the material must be reduced to a minimum. These requirements are satisfied by absorbers having small Z, such as Be, $(CH_2)_2$, and LiH.

Let us consider the application of the absorber method to the production of an enriched beam of K^+ mesons [5]. A diagram of this beam is shown in Fig. 1. A beam of 400 MeV/c π and K mesons, emitted from the target at an angle of 35°, enters a magnet M_1. In addition to separating the required momentum interval this magnet also focuses the beam onto a beryllium absorber.* The thickness of the absorber is 8 cm. After passing through the absorber, the beam enters a second magnet M, which separates the K and pions in space. The separation coefficient is equal to 50.

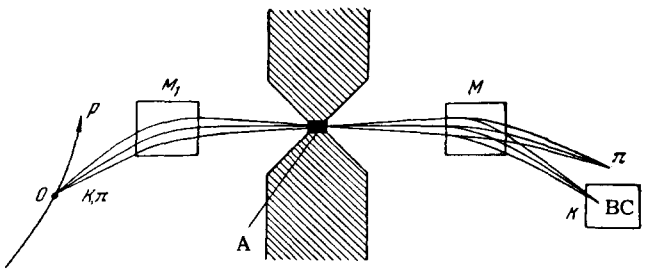

FIG. 1. Diagram of a 400 MeV/c K-meson channel. O—target; p—beam of accelerated protons; K, π—beam of particles to be separated; M_1, M—deflecting and focusing magnets; A—beryllium absorber; BC—bubble chamber.

A recent paper [6] reports a projected separator with which to obtain an enriched beam of antiprotons and K mesons with momentum up to 6 GeV/c. The authors believe that a beam with a π-meson, K-meson, and antiproton ratio of 1 : 8 : 8 can be obtained if a momentum interval $\Delta p/p = 0.25\%$ can be attained for the separated particles, and if the current stability in the magnets and lenses is on the order of 0.01%. The moderator proposed is solid $(CH_2)_2$.

The simplicity of the absorber method will apparently continue to attract the attention of physicists in the future, particularly in those cases when a low admixture of background particles is not essential.

2. Muon Beams

Muons are produced predominantly by pion decay

$$\pi^{\pm} \longrightarrow \mu^{\pm} + \nu.$$

*If the beam is focused on an absorber the particle scattering exerts a smaller influence on the quality of separation.

Research with muons without special measures is very difficult, because of the low intensity and the large background of the strongly-interacting pions. This raises the problem of producing high-intensity muon beams with a low pion admixture.

The muons produced by decay of high-energy pions are concentrated in a cone with an apex angle $2\theta_{max}$, defined by the relation [7]

$$\sin\theta_{max} = \frac{E_{0\pi}^2 - E_{0\mu}^2}{2E_{0\mu}p_\pi c}, \qquad (2.3)$$

where $E_{0\pi}$ = 140 MeV is the rest energy of the decaying pions, p_π their momentum, and $E_{0\mu}$ = 106 MeV is the rest energy of the muons.

The momenta p_μ of the produced muons, depending on their angle of emission, are given by [7]

$$p_\mu c = \frac{E_\pi^* \beta_\pi \cos\theta \pm \sqrt{E_\pi^{*2} - E_{0\mu}^2 \gamma_\pi^2 (1 - \beta_\pi^2 \cos^2\theta)}}{\gamma_\pi (1 - \beta_\pi^2 \cos^2\theta)}, \qquad (2.4)$$

where we introduce the notation

$$E_\pi^* = \frac{E_{0\pi}^2 + E_{0\mu}^2}{2E_{0\pi}}$$

for the energy of the pions in the c.m.s., and γ_π for their energy in the laboratory system divided by the rest energy.

The distance over which the intensity of the pions decreases as a result of the decay by a factor e is equal to

$$L = \frac{\tau p_\pi c^2}{E_{0\pi}}, \qquad (2.5)$$

where $\tau = 2.65 \times 10^{-8}$ sec is their lifetime. To obtain an intense muon beam it is obviously necessary to gather the muons within a distance comparable with the decay length (2.5). This problem can be solved by producing a strong-focusing channel consisting of a set of quadrupole lenses. A detailed calculation of the optical properties of the channel and of the measurement of the characteristics of the employed lenses can be found in several papers [8-10]. Since the muons are produced over the entire length of the channel, the number of lenses required to shape the beam, and accordingly the power consumed, is quite appreciable. With increasing pion momentum the length of the channel increases greatly and the economic factors become the main obstacles. This difficulty can be eliminated to some degree by using in place of lenses a recently proposed system, consisting of several parallel conductors carrying a strong current [11]. Such a system, as shown by the authors of [11], is capable of retaining a considerable fraction of the produced muons.

At present there is a report of only one muon channel in operation [12]. This channel (Fig. 2), constructed at CERN, yields muon beams of high energy (from pions in the momentum region ~430 MeV/c) and low energy (pions with momentum above 230 MeV/c and accordingly muons with momentum 130 MeV/c and below). By way of an example we cite the

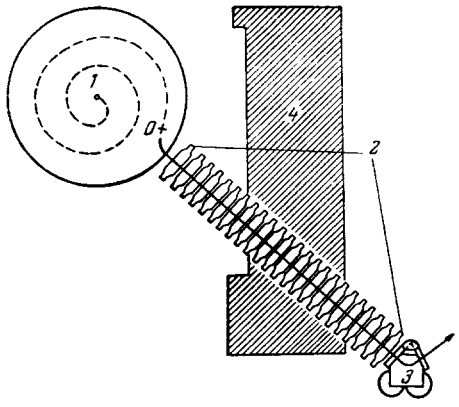

FIG. 2. Schematic diagram of the CERN muon channel. 1–Synchrocyclotron, 2–optical channel of quadrupole lenses, 3–analyzing magnet, 4–concrete shield.

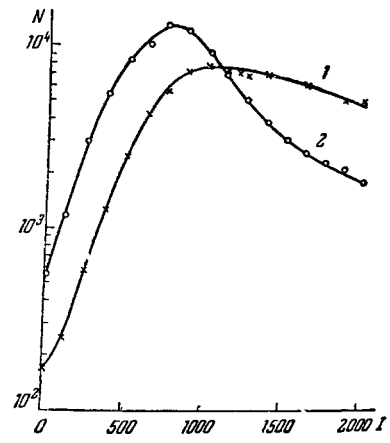

FIG. 3. Dependence of the meson intensity N on the lens currents I (in amperes) in the CERN muon channel. Curve 1–high-energy mesons, curve 2–low-energy mesons.

characteristics of the muons produced at high energies. For pions with momentum 420 MeV/c we have E_π = 440 MeV, E_π^* = 116 MeV, $\beta_\pi \simeq 0.954$, and γ_π = 3.14. Starting from relations (2.3)—(2.5), we obtain for the muons in this case $\theta_{max} \simeq 100$ mrad, $p_{\mu\,max} \simeq 424$ MeV/c, $p_{\mu\,min} \simeq 235$ MeV/c and L ≃ 24 meters. It is clear therefore that the main difficulty in the production of the channel is to ensure an optimal muon yield in the presence of an extended source, with rather large angle and energy values, which is still unusual for optical systems. In order to shape the muon beams, 24 quadrupole lenses are used in the channel, arranged on a base 13 meters long. The lens aperture is 20 cm, and the maximum magnetic field gradient attained in the lens is 1,000 Oe/cm.

The source of the pions entering the channel is a beam of protons accelerated in a synchrocyclotron to 600 MeV. The initial momentum analysis of the pions is by the field of the accelerator itself, which separates the particles with momenta 350 MeV/c and higher. To obtain a low-energy muon beam it is necessary to reverse the direction of the accelerator magnetic field, so that the protons are accelerated in the opposite direction. Then, by suitable choice of the target position, pions with a momentum interval in the 230 MeV/c region will enter the channel. The final momentum analysis is by a strong-focusing magnet consisting of three sections and turning the particle through 70°. The magnet weighs 21 tons. The average radius of curvature if 110 cm, and the maximum field on this radius reaches 10,000 Oe. From the focusing point of view the magnet is a continuation of the channel. The channel is adjusted by varying the currents in the lenses. The dependence of the meson intensity on the current settings is shown in Fig. 3.

Measurements made in the channel have shown that, at a momentum of 280 MeV/c, 4300 μ^- mesons strike every second a 10 × 10 cm target located 110 cm from the magnet. The momentum scatter in the beam is ± 6.3% at half-height of the curve, and the angle scatter relative to the beam axis at the same place is ± 27 mrad horizontally and ± 60 mrad vertically. The pion background reaches 1.5%. At a distance of 80 cm from the magnet the intensity increases to 6,000 negative muons per second, and the pion background reaches 2.2%. These figures have been obtained with a 0.25 μA proton beam accelerated to final energy.

3. Neutrino Beams

For investigations of weak interactions in which neutrinos take part it is necessary to obtain intense beams of these particles. The cross section for the interaction between neutrinos and matter is negligibly small ($\sigma \simeq 10^{-38}$ cm^2) [13]. Very thick absorbers (steel or concrete) are therefore used to separate the background. Owing to the small interaction cross section, a neutrino beam passes through the absorber with practically no attenuation, whereas the corresponding background is considerably absorbed.

High-energy neutrino beams are obtained in large accelerators essentially by decay of π and K mesons:

$$\pi^\pm \to \mu^\pm + (\nu_\mu,\ \tilde{\nu}_\mu),$$
$$K^\pm \to \mu^\pm + (\nu_\mu + \tilde{\nu}_\mu).$$

A high intensity neutrino beam can be obtained by focusing the π and K mesons in a wide momentum and emission-angle interval. The latter circumstance is important, since the neutrinos produced when these particles decay have a narrow angular distribution. To focus the neutrino, a special device—a "magnetic horn" [14]—is used at CERN. Its operating principle can be best illustrated with an example taken from geometrical optics. Assume that we

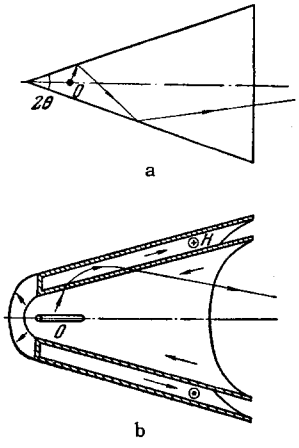

FIG. 4. Magnetic horn. a) Optical analog of magnetic horn; b) construction of horn.

have a cone with apex angle 2θ and a totally reflecting internal surface (Fig. 4a). If we place somewhere on its axis a light source O, then such a system focuses the rays in the axial direction. A similar property with respect to charged particles of the same sign is possessed by the magnetic horn if the particles are produced in a target placed on the axis inside the horn. The arrangement of the horn is shown schematically in Fig. 4b. Current flows in opposite directions through two concentric conducting cones. A strong magnetic field, inversely proportional to the distance from the axis, is produced in the space between the cones. The particles emitted from the target pass through the wall of the internal cone, enter the magnetic field, and are focused there in the direction of the horn axis. The calculated particle trajectories are given in [15]. The maximum emission angle at which the particles can still be focused by the magnetic horn depends on the horn dimensions, magnetic field intensity, and momentum. To focus particles with large momenta, on the order of several GeV, exceedingly large currents are necessary (hundreds of kA), which can be obtained only by pulsed operation of the horn. The pulse duration in this case is on the order of 200 microseconds.

The mechanical stresses that occur during the operation of the horn reach several tons, and the temperature of the internal conductor is raised 70°C following each pulse. All this imposes stringent requirements on the choice of the material of the internal cone, particularly its narrow part. Tantalum was chosen for its good mechanical properties. The target placed inside the horn was a cylindrical rod of heavy material (tungsten) 15 cm long and 5 mm in diameter. The small target diameter has made it possible to extract from it pions and K mesons at small emission angles. This, however, raises the problem of focusing the proton beam extracted from the accelerator onto a target of very small transverse dimensions. This problem is solved by using

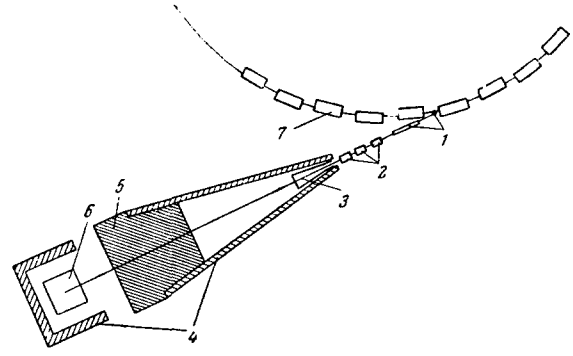

FIG. 5. General schematic diagram of the neutron channel of CERN. 1 – deflecting magnets, 2 – quadrupole lenses, 3 – magnetic horn, 4 – concrete shield, 5 – steel absorber, 6 – bubble or spark chamber, 7 – accelerator.

magnetic quadrupole lenses. To improve the background conditions during the registration of the neutrino interaction, fast single-turn extraction of the beam from the accelerator is used. A diagram of the CERN neutrino channel is shown in Fig. 5. It is used at present for research with a neutrino beam.[16] A total of 332,000 bubble-chamber photographs have already been obtained. The experiments are carried out with protons accelerated to 24.8 GeV, and 7×10^{11} protons are delivered to the target in the magnetic horn in each pulse.

III. ELECTROSTATIC SEPARATORS

1. Principle of Electrostatic Separation

The mass separation of secondary particles in an electrostatic field is based on very simple considerations. Particles with identical momenta but with different masses differ in velocity by Δv. When moving through a homogeneous electric field perpendicular to their motion, such particles acquire unequal transverse momenta, owing to the difference in the transit time through the field region, and leave the field at different angles. This makes it possible to separate in space beams of secondary particles by species (by masses). Instruments making use of this principle for the separation of particle beams of one species are called electrostatic separators.

Let us now consider the quantitative aspect of this separation method [17]. Let particles of two species with identical momentum p and different velocities β_1 and β_2 move in the direction of the z axis, and let a homogeneous electric field of intensity $\mathscr{E}$ be directed along the x axis. Then the equation of motion in the x direction can be written in the form

$$\frac{dp_\perp}{dt} = e\mathscr{E}, \tag{3.1}$$

where $p_\perp$—transverse momentum and e—particle charge. For initial conditions

$$p_\perp(0) = 0 \tag{3.2}$$

we obtain

$$p_\perp = e\mathcal{E}\tau, \tag{3.3}$$

where τ—time of flight through the region with the field. If the length of this region along the z axis is l, then $\tau_{1,2} = l/c\beta_{1,2}$. It is assumed henceforth that $p_\perp \ll p$. The difference in the transverse momenta of these particles is given by

$$\Delta p_\perp = \frac{e\mathcal{E}l}{c}\Delta\left(\frac{1}{\beta}\right), \tag{3.4}$$

where $\Delta(1/\beta) = 1/\beta_1 - 1/\beta_2$. The angle $\Delta\alpha$ between the particle trajectories on leaving the field region is equal to $\Delta p_\perp/p$, or, taking (3.4) into account

$$\Delta\alpha = \frac{e\mathcal{E}l}{pc}\Delta\left(\frac{1}{\beta}\right). \tag{3.5}$$

For the extremely relativistic case, when $\beta_1 \simeq \beta_2 \simeq 1$, we have

$$\Delta\left(\frac{1}{\beta}\right) \approx -\frac{\Delta(E_0^2)}{2(pc)^2}, \tag{3.6}$$

where $\Delta(E_0^2) = E_{01}^2 - E_{02}^2$ (E_{01} and E_{02}—rest energies of the particles in question). Substituting (3.6) in (3.5) we get

$$\Delta\alpha = -\frac{e\mathcal{E}l}{2(pc)^3}\Delta(E_0^2). \tag{3.7}$$

The linear separation of the beams in the separation plane y = 0 is, in accordance with (3.7), equal to

$$\Delta x = -\frac{e\mathcal{E}l\Delta(E_0^2)}{2(pc)^3}\left(\frac{l}{2} + L\right), \tag{3.8}$$

where L is the length along the z axis, transversed by the particles after leaving the field region. It is frequently convenient to retain the initial trajectory of the required species of particles, for example those having a velocity β_1. This can be done by using a homogeneous magnetic field directed along the y axis satisfying the relation [1,18,20]

$$H = \frac{\mathcal{E}}{\beta_1}; \tag{3.9}$$

then the background particles of velocity β_2 acquire a momentum $(p_\perp)_2 = \Delta p_\perp$ in accordance with (3.4). Indeed, the equation of motion is written in this case in the form

$$\frac{dp_\perp}{dt} = e(\mathcal{E} - \beta H). \tag{3.10}$$

For the required particles the Lorentz force is equal to zero. When condition (3.2) is taken into account we have $(p_\perp)_1 = 0$. For the background particle, Eq. (3.10) is written in the form

$$\frac{d(p_\perp)_2}{dt} = e\mathcal{E}\left(1 - \frac{\beta_2}{\beta_1}\right),$$

and consequently the acquired transverse momentum will agree with (3.4).

An essential factor in this method is that the beam separation $\Delta\alpha$ is inversely proportional to the cube of the particle momentum. This circumstance, as will be shown below, imposes a limit on the use of this principle at very high particle energies.

2. Schematic Diagram of Electrostatic Separator

The schematic diagram of the electrostatic separator is shown in Fig. 6a. The optical source of secondary particles is the target O. The solid angle of the separator is determined by a system of collimators K_1. The secondary particles emitted from the target pass through collimators K_1, are focused by the magnetic objective Q_1, and enter the analyzing magnet M. After magnetic analysis in a horizontal plane (henceforth called the analysis plane), the particles with specified momentum p are focused by objective Q_2 onto the vertical slot of the collimator K_2, forming an intermediate image O′ of the source O. The employed particle-momentum interval $\Delta p/p$ is determined by the width of the slit of this collimator. The intermediate image O′ is in the focal plane of the objective Q_3, from which the parallel beam goes in the direction of the Oz axis through a deflector D, in which static homogeneous fields $\mathcal{E}$ and H are produced.

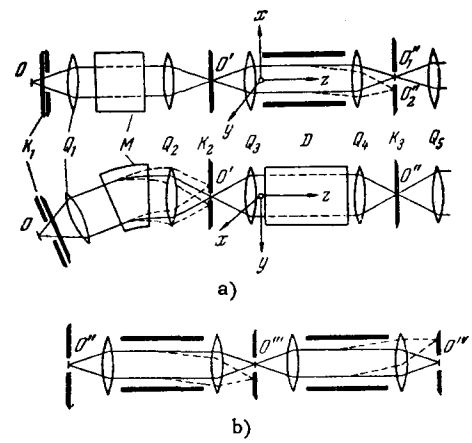

FIG. 6. General schematic diagram of an electrostatic separator: a) single stage, b) two stage, In case a) the separator is depicted both in the separation plane (upper diagram) and in the analyzing plane (lower diagram).

$\mathcal{E}$ is directed along the x axis and H along the y axis, with $\mathcal{E}/H = \beta_1$. Accordingly, the separation of the particles occurs in the vertical plane (henceforth called the separation plane). The particle separation angle $\Delta\alpha$ is determined by (3.5). The images O_1'' and O_2'', produced by the particle beams of different species, are spatially separated in the focal plane of the magnetic objective Q_4. The required particles pass through the collimator slot of collimator K_3 and enter the bubble chamber after focusing. The background particles do not pass through the collimator K_3.

We introduce a coefficient of separation quality

$$\varepsilon = \frac{S}{h''}, \tag{3.11}$$

where S—distance between the centers of the intermediate images O_1'' and O_2'', and h″—their linear dimensions in the separation plane y = 0. In order for the images O_1'' and O_2'' to be minimal, the coeffi-

cient of magnification of the optical system is chosen to be close to unity. Then the dimensions of O_1'' and O_2'' are determined both by the dimensions of the source O itself and by the distortion introduced by spherical and chromatic aberrations of the magneto-optical system. For an ideal optical system (without aberrations) with unity magnification, the dimensions of the images in the separation plane h″ are equal to the height of the target h, and consequently

$$\varepsilon = \frac{S}{h}. \tag{3.12}$$

$S = \Delta\alpha F$, where $\Delta\alpha$ is given by (3.5) and F is the focal distance of the lens.

Consequently

$$\varepsilon = \frac{e\mathscr{E}l}{c}\left(\frac{1}{\beta_1} - \frac{1}{\beta_2}\right)\frac{F}{h}. \tag{3.13}$$

As shown by experience in bubble chamber operation, the beam can be separated if the following condition is satisfied

$$\varepsilon \geqslant 2. \tag{3.14}$$

In practice account must be taken of different aberrations in the optical system, and of other disturbing factors not connected with the optics (we shall stop to discuss them in greater detail below). As a result, the images O_1'' and O_2'' become smeared out and may overlap, i.e., the particle separation is incomplete. Several deflectors are therefore usually included in the separator, and when the beam of the required particle passes through these deflectors it is gradually "cleared" of the background.

Figure 6b shows a two-stage separator of this type. As will be shown below, the optical magnification of each stage is chosen close to minus unity, i.e., each succeeding image is inverted with respect to the preceding one. Since most background particles are located on the edge of the optical image of the required particles, better separation conditions are ensured by reversing the signs of $\mathscr{E}$ and H in each succeeding stage relative to the preceding stage.

3. Ion-Optical Separator System

In separators the focusing objectives used are sets comprising several quadrupole lenses (doublets or triplets). A single quadrupole lens cannot produce a real image, for when it focuses in one plane (say, vertical) it defocuses in the other plane (horizontal).

We shall define as the period of the optical system of the separator that part of the optical system contained between two neighboring intermediate images O^{n-1} and O^n. For example, in the separator shown in Fig. 6b, this period is the section between O″ and O‴ (or O‴ and O^{IV}) and is made up of two lenses. Let us design an optical system of this type. We take the simplest objectives (doublets of quadrupole lenses) and carry out the analysis in the "thin" lens approximation. We use the matrix method [21,22] and introduce the vector

$$\mathbf{r} = \begin{pmatrix} x \\ \alpha \\ y \\ \chi \end{pmatrix}, \tag{3.15}$$

characterizing the position of the particle, where x and α are the coordinate and angle of the particle in the vertical plane, while y and χ are the coordinate and angle in the horizontal plane.

If M is the transformation matrix for a single lens, then the position $\mathbf{r}_2$ of the particle after passing through the lens can be represented in the form

$$\mathbf{r}_2 = M\mathbf{r}_1, \tag{3.16}$$

where $\mathbf{r}_1$ is the vector at the input of the lens. For a magnetic quadrupole the transformation matrix is

$$M = \begin{pmatrix} M_x & 0 \\ 0 & M_y \end{pmatrix}, \tag{3.17}$$

$$M_x = \begin{pmatrix} 1 & \frac{d}{2} \\ 0 & 1 \end{pmatrix}\begin{pmatrix} 1 & 0 \\ +\frac{1}{F} & 1 \end{pmatrix}\begin{pmatrix} 1 & \frac{d}{2} \\ 0 & 1 \end{pmatrix} \tag{3.18}$$

in the vertical plane and

$$M_y = \begin{pmatrix} 1 & \frac{d}{2} \\ 0 & 1 \end{pmatrix}\begin{pmatrix} 1 & 0 \\ -\frac{1}{F} & 1 \end{pmatrix}\begin{pmatrix} 1 & \frac{d}{2} \\ 0 & 1 \end{pmatrix} \tag{3.19}$$

in the horizontal plane; $F = \pm H\rho/dG$—focal distance, $H\rho$—magnetic rigidity of the particles, G—gradient of the magnetic field of the lens, d—effective length of the lens. The introduced approximation, in the form of (3.18) and (3.19), is sufficiently accurate if $|F| \gg d$. From the spectra of the matrix M [see (3.17)] we see that the vectors $\binom{x}{\alpha}$ and $\binom{y}{\chi}$ transform independently. We shall henceforth confine ourselves to particle motion in the vertical plane only, since the corresponding horizontal motion is obtained by replacing F with −F in the matrices of all the lenses. As was shown in the preceding section, the employed system of two identical objectives, i.e., the period, successively transforms a point source into a parallel beam and then the parallel beam into a point. Mathematically this process is represented by introducing for the period a transformation matrix T which is the product of three matrices: the transformation matrix for the first objective

$$R = \begin{pmatrix} R_{11} & R_{12} \\ R_{21} & R_{22} \end{pmatrix}, \tag{3.20}$$

the matrix for the space between the objectives with length D

$$Q = \begin{pmatrix} 1 & D \\ 0 & 1 \end{pmatrix} \tag{3.21}$$

and the matrix for the second objective, which is the inverse of R and has the form

$$\overline{R} = \begin{pmatrix} R_{22} & R_{12} \\ R_{21} & R_{11} \end{pmatrix}. \tag{3.22}$$

If the source is situated on the axis of the system at the point z = 0, and the planes $z = z_1$ and $z = z_2$ coincide respectively with the principal planes of the first and second lenses of the first objective then, as shown in [22],

$$\left.\begin{aligned} R_{11} &= 1+\frac{z_2-z_1}{F_1}, \quad R_{12} = z_2+\frac{z_1(z_2-z_1)}{F_1}, \\ R_{21} &= \frac{1}{F_1}+\frac{1}{F_2}+\frac{z_2-z_1}{F_1F_2}, \\ R_{22} &= 1+\frac{z_1}{F_1}+\frac{z_2}{F_2}+\frac{z_1(z_2-z_1)}{F_1F_2}, \end{aligned}\right\} \quad (3.23)$$

where F_1 and F_2 are the corresponding focal distances of the lenses. In order for the matrix R to describe the transformation of a pointlike source into a parallel beam, and for $\bar{R}$ to describe respectively the inverse transformation, the condition $R_{22} = 0$ must be satisfied. If the focal distances are chosen in the following manner:

$$\left.\begin{aligned} F_1 &= \pm z_1\sqrt{1-\frac{z_1}{z_2}}, \\ F_2 &= -\frac{z_2}{z_1}F_1 = \mp z_2\sqrt{1-\frac{z_1}{z_2}}, \end{aligned}\right\} \quad (3.24)$$

then the indicated condition [see (3.23)] is satisfied for both vertical and horizontal motion. Recognizing that Det R = 1 and $R_{22} = 0$, i.e., $-R_{12}R_{21} = 1$, we obtain T in the form

$$T=\begin{pmatrix} 0 & R_{12} \\ R_{21} & R_{11} \end{pmatrix}\begin{pmatrix} 1 & D \\ 0 & 1 \end{pmatrix}\begin{pmatrix} R_{11} & R_{21} \\ R_{21} & 0 \end{pmatrix}=\begin{pmatrix} -1 & 0 \\ -\frac{2R_{11}}{R_{12}}+\frac{D}{R_{12}^2} & -1 \end{pmatrix}.$$

From this we get for the optical magnification of the system

$$T_{11} = -1.$$

An important characteristic of particle separators is the intensity of the resultant beam, which is determined, in particular, by the solid angle of the optical system. If the maximum angle is α in the vertical plane, and χ in the horizontal plane, then the solid angle of the system is

$$\Omega = 4\alpha\chi.$$

The value of α is determined by the vertical dimensions 2a of the aperture of the lens and its position relative to the source:

$$\alpha = \frac{a}{z_1}.$$

In the horizontal plane, the maximum angle is

$$\chi = \frac{b}{R_{12}},$$

where 2b is the horizontal dimension of the lens aperture. According to (3.23) and (3.24)

$$R_{12} = z_2\left(1+\sqrt{1-\frac{z_1}{z_2}}\right).$$

Consequently the solid angle is

$$\Omega = \frac{4ab}{z_1z_2\left(1+\sqrt{1-\frac{z_1}{z_2}}\right)}.$$

When we proceed to consider real optical systems, we must take into account various types of optical aberrations which lead to spreading of the image. The most important contribution is made by chromatic aberration. It is due to the dependence of the optical strength of the lens on the particle momentum and imposes the limitation on the choice of the momentum interval of the separated beam. For a triplet of quadrupoles, the chromatic aberration can be reduced compared with that of a doublet [22]. For greater reduction of this aberration, more complicated magnetic lens—sextupoles—are used [23].

Nonlinear aberrations connected with the higher spatial harmonics in the quadrupole field result in a dependence of the focusing properties of the lens on the coordinates of its aperture. It has been eliminated to a considerable degree in the latest and most improved lenses.

Spherical aberration due to large particle-trajectory angles is in practice negligibly small for high-energy beams, since the angles are always small in this case ($\lesssim 10^{-2}$ rad). Other optical distortions may be due to the instability of the current in the lenses in the presence of stray magnetic fields. The influence of these factors can however, be reduced to a minimum.

4. Example of an Existing Separator

At the present time there are several electrostatic separators in operation in various laboratories [1,18-20,24-29]. Let us stop to discuss in detail a separator for 1.17-GeV/c K^- mesons [1,20], used for several years for bevatron experiments.* A diagram of this separator is shown in Fig. 7. The total length of the channel from the target to the hydrogen bubble chamber is 33 meters. Such a distance accommodates four K^--meson decay lengths, as a result of which only 1.9% of the initial number of K^- mesons enter the bubble chamber. At the entrance to the channel the ratio K^-/π^- is 0.007. To make this ratio at the output of the separator not worse than unity, the separation coefficient (the ratio of the number of sought particles to the background particles at the output of the channel in the presence of separation, divided by the same quantity without the separation), should be of the order of 10^4. This condition is satisfied in a two-stage system.

The position of the target is chosen to make the secondary particles, which are emitted from the target with a specified momentum 1.17 GeV/c at

*There are now more highly perfected systems, and others are being designed[30-32].

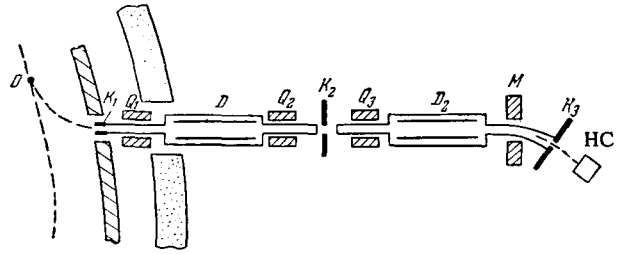

FIG. 7. Diagram of existing bevatron electrostatic separator for 1.17-GeV/c K^- mesons. O–internal target; K_1, K_2, K_3–collimators; Q_1, Q_2, Q_3–quadrupole-lens objectives; D, D_2–deflector; M–analyzing magnet; HC–hydrogen chamber.

zero angle, reach precisely the entrance to the channel. The magnetic analysis of the secondary beam is by the bevatron field. The particles passing through the thin exit window of the accelerated chamber and through the collimator system are focused by the objective into a parallel beam and strike the first deflector. Further motion of the beam is in accordance with the diagram of Fig. 6, except that a deflecting magnet is used at the output of the second deflector for vertical focusing. The final separation of the background particles from the required ones is by collimator K_3.

Let us stop to discuss in greater detail some of the most important details and units of the separator.

Target. The chosen target dimensions are 3.2 × 12.5 × 75 (height, radial dimension, and length along the proton motion, in millimeters). The target material is aluminum. Experiment has shown that approximately 7% of the primary proton beam interacts in such a target. The solid angle of the separator is 4.3 msr. The chosen particle-momentum interval $\Delta p/p$ is 2.5%, thus ensuring a K^--meson flux 0.87 $K^-/10^{10}$ protons at the entrance to the hydrogen chamber.

Deflectors. The transverse cross section of the deflector is shown in Fig. 8. The horizontal homogeneous compensating magnetic field is produced by longitudinal winding. Walls A and B of the iron housing serve as the pole surfaces, while E and F serve as the magnetic core. The upper and lower stainless-steel bases C and D ensure complete vacuum isolation of the internal part of the deflector. Each electrode is approximately 6 meters long and 17.5 cm wide, and is mounted on a metal frame. The distance between the electrodes is 5.5 cm. The electrodes are stainless steel.

The working voltage is 380 kV, with a magnetic field intensity 216 G, thus satisfying the condition $\mathscr{E}/H = \beta$. The K-meson and pion separation angle is 2.32 mrad. To obtain K^- mesons with a small admixture of background particles it is important to attain high homogeneity and stability of the electric and magnetic fields. The stability of the electric field is maintained within 1%, and that of the magnetic field

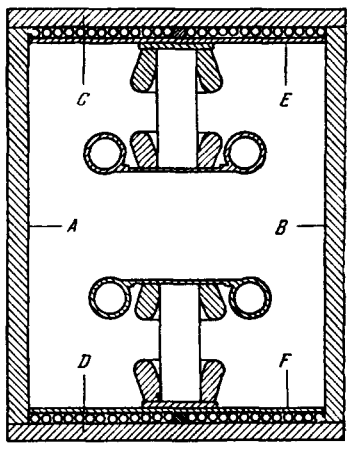

FIG. 8. Construction of the deflector (cross section).

within 0.34%. The mean square deviation of the gap between the electrodes does not exceed 0.02 mm over the entire surface.

Beam optics. The objectives Q_1, Q_2, and Q_3 are quadrupole triplets. Measurements have shown that the most dangerous aberration in this installation is the nonlinear aberration. In DFD (defocusing + focusing + defocusing lenses) objectives the aberration is much smaller than in FDF objectives. For the vertical focusing, which must satisfy more stringent requirements, all three objectives are therefore of the DFD type, although the chromatic aberration is in this case higher. Type FDF objectives are used to focus the beam in the horizontal plane.

Separation efficiency and background. There are many causes for the spreading of the intermediate images and for the appearance of background particles in the K^--meson image. The most important among them are: (1) nonlinear and chromatic aberrations in the focusing quadrupoles, (2) multiple scattering of the particles as they pass through the accelerator-chamber exit window which separates the vacuum system of the bevatron from the vacuum system of the separator. (3) "halo" due to the decay of the pions and strange particles in the target region, (4) production of particles on the target holder, (5) inhomogeneity and instability of the magnetic field of the accelerator along the trajectory from the target to the exit window, (6) scattering of the particles on the edges of the collimator slot, (7) instability and inhomogeneity of the fields in the deflectors and lenses, and (8) $\pi \rightarrow \mu$ decay in the channel, which leads to a contamination of the beam by muons. The muon background can be appreciable, since the deflector does little to separate the muons from the K^--mesons, owing to the fact that the average $\pi \rightarrow \mu$ decay angle is considerably larger than the separation angle, so that the percentage of contamination by muons is determined by the probability of their

striking the slots of the collimators K_2 and K_3. For the second stage, factors (2)—(5) drop out. Therefore, as expected, the separation coefficient in the second stage is one order of magnitude higher. The over-all separation coefficient is 10^5, and the K^-/π^- ratio at the entrance to the bubble chamber is 12.5.

5. Field of Application of the Electrostatic Separation Method

Further progress in separator construction technology has made it possible to obtain pure beams with higher energies than in the example of the working separator shown. Thus, there is in operation at CERN a two-stage separator [3] which yields pure beams of 3.5-GeV/c K^- mesons, 5-GeV/c antiprotons, and 6-GeV/c π^+ mesons. The total channel length from the target to the bubble chamber is 87 meters. The field intensity in each stage is $\mathscr{E}$ = 50—60 kV/cm. Separators are also under construction at CERN and other laboratories for higher antiproton momenta (up to 6 GeV/c)[31,32]. The lengths of these channels amount to hundreds of meters, and the electric field intensities in the deflectors reach 100 kV/cm. Such marked progress is due principally to improvement in the optical systems of the channels. The dimensions of the images in the separation plane have been reduced to 1—2 mm, the chromatic aberration has been decreased as a result of using sextupoles and other systems, while the remaining types of aberrations and distortions in the optical systems have been eliminated to a considerable degree. It can be stated that the improvement in the optics has reached its practical limit and further progress can be obtained only by improving other parameters. In accordance with (3.6) and (3.13), the separation quality coefficient for ultra-relativistic energies and for optimal optics is

$$\varepsilon = \frac{elV(E_{02}^2 - E_{01}^2)}{2(pc)^3 A}, \qquad (3.25)$$

where V = $\mathscr{E}$s—total voltage on the deflector electrodes, A = hs/F—acceptance of the beam in the separation plane, and s—gap between the deflector electrodes. For example, when working with bubble chambers it is still possible to attain ε = 2. In accordance with (3.25), for this case the limiting momentum of the separated particles $(pc)_{max}$ is equal to

$$(pc)_{max} = \left(\frac{E_{02}^2 - E_{01}^2}{4}\frac{eVl}{A}\right)^{1/3}. \qquad (3.26)$$

It follows therefore that higher energies in electrostatic separation can be attained as a result of the following: (a) reduction in the acceptance A, (b) increase in the voltage V on the deflector electrodes, and (c) increase in the length of the deflector l. Let us discuss each of these possibilities [23,33,34].

The vertical acceptance of modern separators reaches a value of 0.1—0.2 mrad-mm at a target height h = 1—2 mm. Any further appreciable decrease is hardly advantageous, for this leads to such a decrease in the intensity of the separated beam that the effective operation of the bubble chamber becomes impossible.

The limiting voltage on the electrodes is determined by the value at which intense breakdowns arise. At present voltages up to 500 kV are used and there are grounds for assuming that this can be raised to 1 megavolt in the future by special treatment of the electrode surface, by choice of material, and by special conditioning. Interest attaches to the construction of electrodes in which the surface of one of the electrodes is covered by polished glass [35]. In the course of operation of the deflector, this glass is specially heated. Such deflectors are already used in existing separators [26], and produced high field intensities ($\simeq$ 100 kV/cm).

The length of the deflector plates in modern separators reaches $\sim$20 meters. Further increase in the length becomes difficult, since account must then be taken of the beam divergence and of the attainability of the specified stability and homogeneity of the electric and magnetic fields. The latter imposes a stringent limitation on the length of the electrodes and determines the limit of utilization of the electrostatic separation method at very high energies. Indeed, the fluctuations of the deflection angle $\delta\alpha$ are connected with the fluctuations of the electric and magnetic fields $\delta\mathscr{E}$ and δH by

$$\frac{\delta\alpha}{\alpha} = \frac{\delta\mathscr{E}}{\mathscr{E}} + \frac{\delta H}{H},$$

where

$$\alpha = \frac{e\mathscr{E}l}{pc\beta}.$$

For normal operation of the separator it is necessary to satisfy the condition

$$\frac{\delta\alpha}{\alpha} \ll \frac{\Delta\alpha}{\alpha},$$

where $\Delta\alpha$ is given by (3.5). Recognizing that for high energies $\beta_1 \simeq \beta_2 \simeq 1$, we obtain a condition for the stability of the fields $\mathscr{E}$ and H:

$$\frac{\delta\mathscr{E}}{\mathscr{E}} \ll \Delta\beta \text{ and } \frac{\delta H}{H} \ll \Delta\beta.$$

Thus, for example, when separating antiprotons and pions with momentum 5 GeV/c, we get $\Delta\beta \simeq 10^{-2}$. It follows therefore that the stability and homogeneity of the fields $\mathscr{E}$ and H should be of the order of 10^{-3}. On the other hand, since

$$\Delta\beta \simeq \frac{E_{02}^2 - E_{01}^2}{2(pc)^2},$$

the stability of the homogeneity must be maintained at a level not worse than 10^4 when the momentum of

the separated particles (antiprotons) is increased from 5 to 15 GeV/c. Such tolerances, particularly for long deflectors, create a very complicated technical problem. The production of pure antiproton beams with the aid of electrostatic separators is apparently limited to momenta not exceeding 15 GeV/c. Accordingly, for K mesons this limit lies in the region 10 GeV/c. When considering the separation of K mesons, account must also be taken of the fact that these are unstable particles and that long channel lengths can lead to a considerable decrease in their number.

IV. ELECTRODYNAMIC SEPARATORS

1. Basic Principles

A new approach to the problem of mass separation of particles is based on ideas connected with the use of the analyzing properties of high frequency (hf) electromagnetic fields. An important factor in the successful development of these principles is the fact that many accelerators produce an accelerated particle beam with a sufficiently good high-frequency structure, i.e., the accelerated beam is modulated in intensity at the frequency of the accelerating voltage. The most instructive in this respect is the linear accelerator. Its output beam constitutes periodically repeating pulses of accelerated particles with a sufficiently high off-duty factor. The secondary particles produced by the interaction between the accelerated beam and the target will obviously duplicate the high-frequency structure of the primary beam. W. Panofsky [36] proposed an original method of mass separation of particles with a linear accelerator, which reduces briefly to the following.

Assume that single-momentum particles of two species are emitted periodically from a target during a short time interval $\Delta t \ll T$, where T is the period of the accelerating voltage. Their position relative to the accelerating voltage at the instant of emission from the target is shown schematically in Fig. 9a. As they traverse the free space, the particles become mass-separated along their trajectories. The heavier particles, with lower velocity, lag the light particles. The separation Δz over a certain base L can be expressed in the form

$$\Delta z = L\left(\frac{1}{\beta_1}-\frac{1}{\beta_2}\right). \qquad (4.1)$$

If we now produce along the path of the particles, in some region of length l, a high frequency electric field having the same wave-length λ as the wavelength of the accelerating field in the linear accelerator, and if $l \ll \lambda$, then the angular deflection of the particles α will be determined only by the instant when the particles enter this region.

If L is chosen such that

$$\Delta z = \frac{\lambda}{2}(2n+1), \qquad (4.2)$$

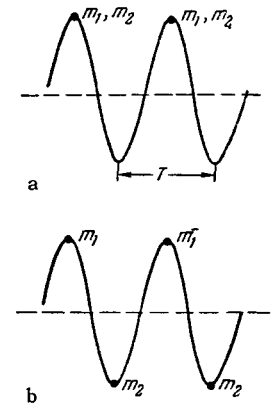

FIG. 9. Positions of the separated particles relative to the high-frequency deflecting field. a) Instant of leaving the target; b) instant of entering the deflecting system (m_1, m_2–particle masses, T–period of the high-frequency deflecting field).

where n = 0, 1, 2, . . . , and the deflecting field has a maximum value at the instant when the light particles enter, the particles under consideration are subjected to angular deflections which are opposite in sign (Fig. 9b), and can subsequently be separated in space. The separation angle is in this case

$$\Delta\alpha = \frac{e\mathcal{E}l}{pc}\left(\frac{1}{\beta_1}+\frac{1}{\beta_2}\right). \qquad (4.3)$$

The deflecting system can be constructed in the form of a single cavity or a system of cavities, and also in the form of a waveguide that produces transverse deflection.

The possibility of spatially separating secondary particles by masses with the aid of waveguides with traveling waves, as applied to linear accelerators, was pointed out also by D. V. Volkov [37].

In 1957 V. I. Veksler and V. A. Petukhov (see [38,39]) proposed a method for mass separation of particles with accelerators such as proton synchrotrons with weak and strong focusing. Let us explain the proposed method using the proton synchrotron of the Joint Institute for Nuclear Research as an example. This proton synchrotron is intended to accelerate protons to 10 GeV. During the acceleration, the beam occupies part of the perimeter of the vacuum chamber. Its angular dimensions at the end of the acceleration are approximately 100°, corresponding to linear dimensions on the order of 70 meters. The individual cluster of secondary particles will be of the same size. We can attempt to use this high frequency structure of the secondary-particle beam for mass separation. However, as can be readily seen from (4.1)—(4.2), the base L needed for the required longitudinal mass separation of the particles depends essentially on the wavelength λ of the accelerating voltage. In the proton synchrotron of the Joint Institute for Nuclear Research, at the end of the acceleration we have $\lambda \approx 200$ meters and the necessary base L for particles having energies of several GeV would amount to several kilometers.

The authors proposed to get around this difficulty by artificially producing the required high frequency structure in the beam of the accelerated protons. This can be done by switching the proton synchrotron to the multiple acceleration mode at the end of the acceleration cycle. Indeed, if the protons are accelerated to their final energy and then the accelerating voltage is turned off, the beam fills uniformly the entire perimeter of the vacuum chamber. If we now apply an accelerating voltage with a frequency q times larger than the frequency of revolution of the beam, and ensure at the same time the required accuracy, we can recapture a considerable fraction of the protons into a new mode—that of multiple acceleration. The accelerated beam will then be bunched in q clusters, and the azimuthal dimension of each will be equal to the wavelength of the multiple voltage $\lambda_q = \lambda/q$, where λ is the wavelength of the accelerating voltage in the normal operating mode of the proton synchrotron. In order to greatly reduce the length of the base L it is necessary to use a multiplicity $q \sim 10^2$. The proton acceleration time at the multiple frequency will be determined only by the time of shaping of the beam and the time of its extraction to the target. The shaped proton clusters are extracted so as to ensure the necessary off-duty factor of the periodically repeating pulses of secondary particles without disturbing the produced high-frequency structure of the circulating beam. The spatial mass separation of the particles occurs at the end of the travel base L and is effected by a system of resonators operating at the same wavelength λ_q.

The hitherto considered dynamic methods of mass separation of particles were based on the presence of the high frequency structure of the separated particle beam. This occurs automatically when working with linear electron accelerators, or else such a structure is produced artificially by switching the accelerator to a multiple acceleration mode. One of the first attempts at dynamic particle separation without a high-frequency beam structure was proposed by J. Blewett [40]. In his method (Fig. 10) a beam of secondary particles of fixed momentum is extracted from the accelerator and guided to a deflector, which comprises a traveling-wave structure in which the propagating electromagnetic wave imparts a transverse momentum to the separated particles. The wave velocity is chosen equal to the velocity of the background particles. The deflector length L satisfies the condition that the required particles change their initial phase by 2π as they move through the deflector. Then we have at the exit from the deflector a diverging beam of background particles and a parallel beam of required particles. The first deflector does not separate the required and background particles completely in space, since part of the background particles is deflected little (π_2 and π_3, case

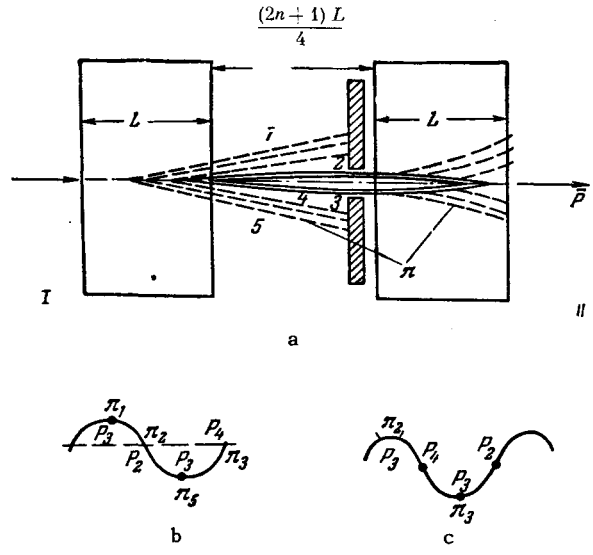

FIG. 10. a) Schematic diagram of high-frequency separator proposed by J. Blewett (I, II–high-frequency deflectors); b) position of separated particles relative to high-frequency fields at the entrance to the first deflector and c) at the entrance to the second deflector.

of Fig. 10a). Complete separation of the particles is effected by the second deflector which has the same dimensions as the first, from which it is separated by a distance

$$\frac{2n+1}{4} L \qquad (n = 0, 1, 2, \ldots). \tag{4.4}$$

In this case the voltage in the second deflector is shifted 180° in phase relative to the first. Now the background particles, which are deflected little, enter the second deflector with phases that contribute to maximum deflection. The necessary particles, which are also shifted 2π in phase in the second deflector, are not deflected again, and consequently can be separated from the background particles.

Developing this idea further, Panofsky proposed to use for separation of the particles a high frequency deflecting electric field with circular polarization [41].

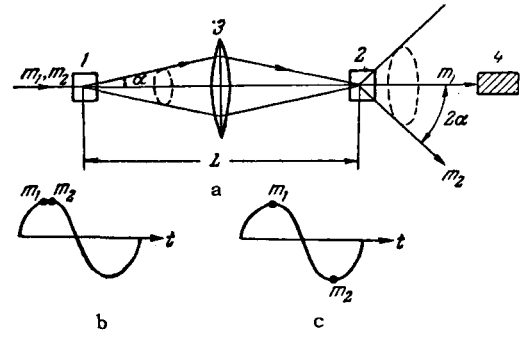

FIG. 11. High-frequency particles separation, proposed by W. Panofsky. a) 1, 2–high-frequency deflectors; 3–system of lenses; 4–absorber. b) position of separated particles relative to the deflecting high-frequency fields at the entrance to the first deflector and c) at the entrance to the second deflector.

Figure 11 shows schematically such a separator, which consists of two identical deflectors separated by a distance L. Between the deflectors is a system of magnetic lenses, which project the center of deflector 1 onto the center of deflector 2. The deflecting electric field of wavelength λ, produced at each deflector, is circularly polarized and its electric vector $\mathcal{E}$ rotates in a plane perpendicular to the axis of the system. The magnitude of this vector and the direction of its rotation are the same in both deflectors. For simplicity we assume for the deflectors lengths $l \ll \lambda$. Let a single-momentum beam with two species of relativistic particles of masses m_1 (background particles) and m_2 (required particles) enter the first deflector. At the exit from this deflector the beam will be distributed over the surface of a cone with apex angle

$$\alpha = \frac{e\mathcal{E}l}{pc}.$$

If the length of the travel base L is

$$L = \frac{\lambda (pc)^2}{E_{02}^2 - E_{01}^2} \qquad (4.5)$$

[see (4.1), (4.2), (3.6)], then at the end of this base the required particles have a phase shift π relative to the background particles. By suitably choosing the phase of the high frequency field in the second deflector, it is possible to suppress completely the deflection which the background particles have acquired in the first deflector, and accordingly double this deflection for the required particles. Thus, at the exit from the second deflector the required particles are distributed over the surface of a cone with apex angle 2α, whereas the background particles form an undeflected parallel beam. An absorber placed at the center intercepts the background particles, and by the same token ensures spatial separation of the initial beam. It must be emphasized that the high-frequency structure of the beam entering the separator can in this case be arbitrary; in particular, the beam can be continuous.

To obtain a circularly polarized high-frequency beam it is obviously necessary to excite simultaneously two ordinary linearly-polarized modes, with mutually perpendicular polarization planes. This can be accomplished by using as the high-frequency deflector, for example, a system of two identical cavities which are mounted flush to each other and are turned 90° relative to each other. It is seen therefore that the power required for this separation method is practically double that of systems that deflect the particles in one plane only. It is precisely for this reason that the main emphasis in Panofsky's scheme is on using high-frequency systems with linearly polarized waves [42-49]. In such systems the particle deflection is in one plane, so that the particles at the exit from the second deflector are concentrated in an angle interval $\pm 2\alpha$ in the plane of polarization of the wave. Although this variant entails a certain loss of intensity of the required particles in the absorber, it is energetically more favorable and much simpler in construction. In addition, it becomes possible in this case to separate the analysis and separation planes, thereby facilitating the production of minimum image dimensions for the separated beams.

All the dynamic methods considered so far have yielded a transverse particle deflection dependent on the longitudinal particle velocity. The longitudinal momenta of the particles of the different species remained practically unchanged. As indicated by Murray [50], particle separation with the aid of high frequency fields can be realized by a different method, reminiscent of the absorber method. As is well known, it is relatively simple to mass-separate particles by the absorber method at low energies. On the other hand, at high energies the method becomes ineffective because of the small difference in the ionization losses of the separated particles. In high-frequency systems it becomes possible to produce a momentum difference between particles of different mass and identical momentum at appreciably larger energies than in the absorber method. To this end Murray proposed a system of the linear-accelerator type (Fig. 12).

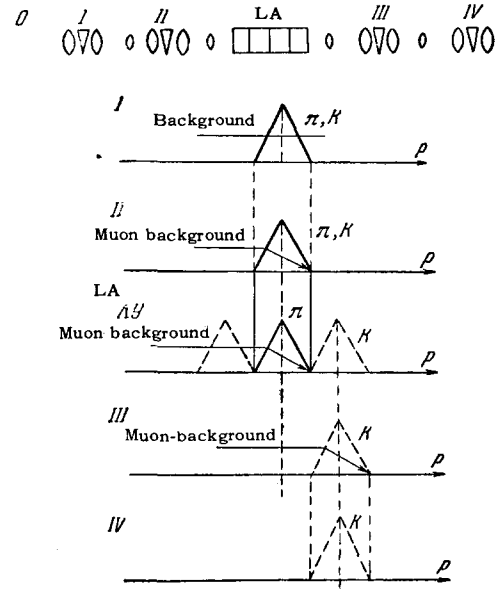

FIG. 12. Diagram of high frequency separator of the accelerating type, proposed by J. Murray. I, II, III, IV—elements of ion-optical system of the separator (magnetic quadrupole lenses, turning magnet); LA—linear accelerator; I, II—momentum distribution of the separated particles and of the background following the passage through the first and second elements of the ion-optical system; LA—after passing through the linear accelerator, III, IV—after the third and fourth elements of the ion-optical system.

The phase velocity of the wave in such a system should be chosen equal to the velocity of the required particles. The length of the system is determined from the condition that the background particles

change their phase 2π on passing through the system. In such a case, part of the required particles will be accelerated. The background particles will acquire no increase in energy whatever. Subsequent magnetic analysis makes it possible to separate the particles by masses.

2. Motion of Charged Particles in High-Frequency Fields

In the preceding section we have shown that in dynamic separators the deflecting elements are either resonators or waveguides. Let us establish the main laws governing the motion of charged particles in such systems. Starting from this analysis, we immediately single out the class of high-frequency structures which can be used for the separation of particles with different masses. We use in our exposition the results of [51,52]. In view of the importance of this question and some specific features of resonator and waveguide systems, we describe the behavior of charged particles in each system separately.

a) Resonator systems. From the point of view of separation of charged particles, greatest interest is attached to the transverse momentum $\mathbf{p}_\perp$ acquired by the particle after passing through the resonator. Let a particle with charge e move along the z axis of a resonator with velocity v_z. In the calculation we assume that the particle velocity v_z does not change on passing through the resonator. Then the momentum $\mathbf{p}_\perp$ acquired by the particle will be given by

$$\mathbf{p}_\perp = \frac{e}{v_z}\int_0^l \left[\mathbf{E}_\perp + \frac{1}{c}[\mathbf{vH}]_\perp\right] dz, \qquad (4.6)^*$$

where l—length of the resonator in the Oz direction. We express E and H in terms of the vector potential A, using the relations

$$\mathbf{E} = -\frac{1}{c}\frac{\partial \mathbf{A}}{\partial t}, \quad \mathbf{H} = \operatorname{rot}\mathbf{A}, \qquad (4.7)^\dagger$$

and using the vector identity

$$\operatorname{grad}(\mathbf{vA}) = (\mathbf{A}\nabla)\mathbf{v} + (\mathbf{v}\nabla)\mathbf{A} + [\mathbf{A}\operatorname{rot}\mathbf{v}] + [\mathbf{v}\operatorname{rot}\mathbf{A}]. \qquad (4.8)$$

Owing to the constancy of z, the values of $\mathbf{A}\times\operatorname{curl}\mathbf{v}$ and $(\mathbf{A}\cdot\nabla)\mathbf{v}$ vanish, and (4.6) takes the form

$$\mathbf{p}_\perp = -\frac{e}{cv_z}\int_0^l \left\{\left[\frac{\partial \mathbf{A}}{\partial t} + (\mathbf{v}\nabla)\mathbf{A}\right]_\perp - \nabla_\perp(\mathbf{vA})\right\} dz, \qquad (4.9)$$

where $\nabla_\perp$—transverse component of the operator ∇, expressed for example, in rectangular coordinates by

$$\nabla_\perp = \frac{\partial}{\partial x}\mathbf{u}_1 + \frac{\partial}{\partial y}\mathbf{u}_2$$

($\mathbf{u}_1$ and $\mathbf{u}_2$ are unit vectors along the corresponding axis).

*$[\nu\mathbf{H}] = \nu \times \mathbf{H}$.

†rot = curl.

Since

$$\frac{\partial \mathbf{A}}{\partial t} + (\mathbf{v}\nabla)\mathbf{A} = \frac{d\mathbf{A}}{dt},$$

we obtain from (4.9)

$$\mathbf{p}_\perp = \frac{e}{c}\left\{[\mathbf{A}_\perp(z=0) - \mathbf{A}_\perp(z=l)] + \int_0^l \nabla_\perp A_z\, dz\right\}. \qquad (4.10)$$

If the end walls of the resonator are perpendicular to the Oz axis, then $\mathbf{A}_\perp$ on these walls coincides with the tangential component of the vector potential A, a component which vanishes on the resonator walls. The first term in (4.10) therefore vanishes and we ultimately have

$$\mathbf{p}_\perp = \frac{e}{c}\int_0^l \nabla_\perp A_z\, dz. \qquad (4.11)$$

In (4.11) we can transform from the vector potential A to the fields by using (4.7). Representing A in complex form $\mathbf{A} = \mathbf{A}_0 \exp(i\omega t)$, we get from (4.11)

$$\mathbf{p}_\perp = \frac{ei}{\omega}\int_0^l \nabla_\perp E_z\, dz. \qquad (4.12)$$

It follows from (4.11) and (4.12), in particular, that the particles exhibit a very important difference in their behavior in high-frequency fields of different types. If TE oscillations are excited in the resonator (there is no E_Z component of the electric field), then, as follows from (4.12), $\mathbf{p}_\perp = 0$, i.e., TE modes are not suitable for separation of charged particles. In this case the effect of the electric field is completely offset by the effect of the magnetic field. Thus, to separate particles it is necessary to use TM modes (no H_Z component of the magnetic field). In order to ascertain the main laws governing the behavior of the particles in TM fields, let us discuss as a specific example a resonator in the form of a rectangular parallelepiped. The natural oscillations in resonators of simplest form were considered in many works (see, for example, [53]). For the TM mode in a rectangular parallelepiped, the components of the vector potential take the form

$$\left.\begin{aligned} A_x &= \frac{A_0\gamma_1\gamma_3}{k}\cos\gamma_1 x\cdot\sin\gamma_2 y\cdot\sin\gamma_3 z\cdot\sin kct,\\ A_y &= \frac{A_0\gamma_1\gamma_3}{k}\sin\gamma_1 x\cdot\cos\gamma_2 y\cdot\sin\gamma_3 z\cdot\sin kct,\\ A_z &= -\frac{A_0(k^2-\gamma_3^2)}{k}\sin\gamma_1 x\cdot\sin\gamma_2 y\cdot\cos\gamma_3 z\sin kct, \end{aligned}\right\} \qquad (4.13)$$

where $\gamma_1 = n_1\pi/a$, $\gamma_2 = n_2\pi/b$, $\gamma_3 = n_3\pi/l$, $k = \omega/c$, A_0—constant, n_1, n_2, n_3—integers, a, b, l—lengths of the sides of the parallelepiped in the corresponding directions. The origin coincides with one of the vertices of the parallelepiped.

Substituting the expression for A_Z in (4.11) and neglecting the displacement of the particle inside the resonator in the transverse direction, we get for $p_\perp^2$

$$p_\perp^2 = \frac{e^2A_0^2(k^2-\gamma_3^2)^2}{c^2\beta_z^2\left[\left(\frac{k}{\beta_z}\right)^2 - \gamma_3^2\right]^2}$$

$$\times (\gamma_1^2 \cos^2 \gamma_1 x \cdot \sin^2 \gamma_2 y + \gamma_2^2 \cdot \sin^2 \gamma_1 x \cdot \cos^2 \gamma_2 y)$$

$$\times \left[(-1)^{n_3} \cos\left(\frac{kl}{\beta_z} + \varphi_0 \right) - \cos \varphi_0 \right]^2, \qquad (4.14)$$

where φ_0 is the initial phase of the oscillations. For convenience in the analysis we assume that the side edges of the parallelepiped are equal ($a = b$) and confine ourselves to a stationary wave with $n_1 = n_2 = 1$, $n_3 = 0$.

Then (4.14) takes the form

$$p_\perp^2 = \frac{e^2 A_0^2 \pi^2 \beta_z^2}{a^2 c^2} \left(\cos^2 \frac{\pi}{a} x \cdot \sin^2 \frac{\pi}{a} y + \sin^2 \frac{\pi}{a} x \cdot \cos^2 \frac{\pi}{a} y \right)$$

$$\times \left[\cos\left(\varphi_0 + \frac{kl}{\beta_z} \right) - \cos \varphi_0 \right]^2. \qquad (4.15)$$

We see therefore that a particle moving along the resonator axis ($x = y = a/2$) acquires no transverse momentum ($p_\perp^2 = 0$). If we expand the trigonometric functions in (4.15) in a series about this point ($x = y = a/2$), we obtain

$$p_\perp^2 \simeq \frac{e^2 A_0^2 \pi^2 \beta_z^2}{a^4 c^2} r^2 \left[\cos\left(\varphi_0 + \frac{kl}{\beta_z} \right) - \cos \varphi_0 \right]^2, \qquad (4.16)$$

where r is the radius measured from the axis ($x = y = a/2$). It follows from (4.16) that the farther away the particle travels from the resonator axis, the larger the momentum it acquires.

Let us also calculate the deflection of the particle in the fundamental wave (1, 1, 0), if it travels through a resonator in a direction perpendicular to the Oz axis, for example parallel to the Ox axis. Carrying out transformations similar to those above, we obtain for the momentum $p_\perp$ acquired by the particle

$$p_\perp = \frac{e}{c} \int_0^a \nabla_\perp A_x \, dx. \qquad (4.17)$$

Since $\gamma_3 = 0$ for the fundamental wave, we have in accordance with (4.13) $A_x = 0$, and consequently $p_\perp = 0$, i.e., in this case the effect of the electric field E_z is offset by the effect of the magnetic field H_y. A similar result is obtained in the case when the particle travels in the direction of the Oy axis.

To separate the particles it is necessary to have a deflecting element in which the particles entering at the same instant of time under different initial conditions acquire identical displacements. As can be seen from an analysis of the particular example, this requirement is not satisfied by a resonator in the form of a rectangular parallelepiped. The same pertains to a cylindrical resonator. The requirements can be satisfied by using resonators of more complicated shape. As a rule these are difficult to calculate and we present only some estimates for one of them, similar to that employed in the deflecting system of the 5-GeV/c antiproton separator [54]. The resonator has an irregular toroidal form and is shown schematically in Fig. 13 where the direction of particle motion is also shown.

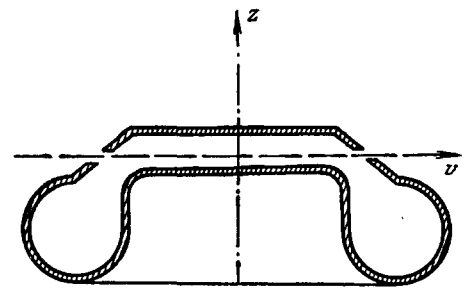

FIG. 13. Form of resonator which serves as the deflecting element for the electrodynamic separator.

Let us consider the case of quasi-stationary oscillations, characterized by the inequalities $\lambda \gg a$, and $\lambda \gg d$, where λ—wavelength of the oscillations, a—radius of the capacitor space, and d—distance between the plates of the capacitor space. If $\lambda \gg d$, the fundamental oscillation in the space where the particle travels takes the form

$$\left.\begin{aligned} E_z &= DJ_0(kr) \cos kct, \\ H_\theta &= -DJ_1(kr) \sin kct, \end{aligned}\right\} \qquad (4.18)$$

where $J_0(kr)$ and $J_1(kr)$ are Bessel functions. For $\lambda \gg a$ we can draw several conclusions with respect to the field in the capacitor space.

1. We can assume for the fundamental mode that E_Z is homogeneous, since

$$J_0(kr) \simeq 1 + \frac{k^2 r^2}{4} \ldots \text{and } ka = \frac{2\pi a}{\lambda} \ll 1.$$

2. The time-averaged energy of the magnetic field concentrated in the capacitor space is much smaller than the average electric energy.

Indeed, their ratio is

$$\frac{\int_V D^2 J_1^2(kr) \, dV}{\int_V D^2 J_0^2(kr) \, dV} \approx \frac{k^2 a^2}{8},$$

where V—volume of the resonator space. This signifies that the magnetic field is almost completely concentrated in the toroidal part of the resonator, which plays the role of a lumped inductance. Since the particle travels in the capacitor space, the influence of the magnetic field on it can be neglected in the first approximation and the momentum $p_\perp$ acquired by the particle will be given by

$$p_\perp = e \int_0^{t_1} E_z \, dt = \frac{eD}{kc} \left[\sin\left(\frac{2ka}{\beta} + \varphi_0 \right) - \sin \varphi_0 \right], \qquad (4.19)$$

where t_1—time of flight through the resonator. Since $ka \ll 1$, for $\beta \simeq 1$, this formula assumes the form

$$p_\perp = \frac{2eDa}{v} \cos \varphi_0. \qquad (4.20)$$

b) Waveguide systems. The derivation of (4.10) is based on the general laws of electrodynamics, and is of course valid for the case considered below. However, to clarify the specific nature of the behav-

ior of the particles in waveguide systems, we present a somewhat different derivation. We assume from the very beginning that the fields are described by expressions

$$\mathbf{E}=\boldsymbol{\mathcal{E}}(\zeta,\ \eta)\,e^{i(\omega t-\varkappa z)},\qquad \mathbf{H}=\boldsymbol{\mathcal{H}}(\zeta,\ \eta)\,e^{i(\omega t-\varkappa z)},\quad (4.21)$$

where $\kappa = \omega/v_\varphi$ is the propagation constant, v_φ is the phase velocity of the wave, and ζ and η are transverse coordinates, which will henceforth take to be rectangular ($\zeta = x$, $\eta = y$). We use Maxwell's equations

$$\left.\begin{aligned} ik\mathbf{E}&=\operatorname{rot}\mathbf{H}, & -ik\mathbf{H}&=\operatorname{rot}\mathbf{E},\\ \operatorname{div}\mathbf{E}&=0, & \operatorname{div}\mathbf{H}&=0\end{aligned}\right\}\quad (4.22)$$

and represent $\boldsymbol{\mathcal{E}}(x, y)$ and $\boldsymbol{\mathcal{H}}(x, y)$ in the form

$$\left.\begin{aligned}\boldsymbol{\mathcal{E}}(x,\ y)&=\boldsymbol{\mathcal{E}}_\perp(x,\ y)+\mathbf{u}_3\mathcal{E}_z(x,\ y),\\ \boldsymbol{\mathcal{H}}(x,\ y)&=\boldsymbol{\mathcal{H}}_\perp(x,\ y)+\mathbf{u}_3\mathcal{H}_z(x,\ y),\end{aligned}\right\}\quad (4.23)$$

where $\mathbf{u}_3$—unit vector along the Oz axis. Writing out (4.22) in terms of its components and taking (4.21) and (4.22) into account, we obtain the following equations relating $\boldsymbol{\mathcal{E}}_\perp$ and $\boldsymbol{\mathcal{H}}_\perp$ with $\mathcal{E}_z$ and $\mathcal{H}_z$:

$$\left.\begin{aligned}[\mathbf{u}_3(\nabla_\perp\mathcal{H}_z+i\varkappa\boldsymbol{\mathcal{H}}_\perp)]&=-ik\boldsymbol{\mathcal{E}}_\perp,\\ [\mathbf{u}_3(\nabla_\perp\mathcal{E}_z+i\varkappa\boldsymbol{\mathcal{E}}_\perp)]&=ik\boldsymbol{\mathcal{H}}_\perp.\end{aligned}\right\}\quad (4.24)$$

Replacing $\boldsymbol{\mathcal{H}}_\perp$ in the first relation of (4.24) by its value from the second relation of (4.24) and vice versa, eliminating $\boldsymbol{\mathcal{E}}_\perp$ from the second expression with the aid of the first, and also using the relation for the double vector product

$$[\mathbf{a}[\mathbf{bc}]]=\mathbf{b}(\mathbf{ac})-\mathbf{c}(\mathbf{ab}),$$

we ultimately obtain

$$\left.\begin{aligned}(k^2-\varkappa^2)\boldsymbol{\mathcal{E}}_\perp&=ik[\mathbf{u}_3\nabla_\perp\mathcal{H}_z]-i\varkappa\nabla_\perp\mathcal{E}_z,\\ (k^2-\varkappa^2)\boldsymbol{\mathcal{H}}_\perp&=-ik[\mathbf{u}_3\nabla_\perp\mathcal{E}_z]-i\varkappa\nabla_\perp\mathcal{H}_z.\end{aligned}\right\}\quad (4.25)$$

As can be readily verified, similar relations also take place in a cylindrical coordinate system.

We now assume that a particle of charge e moves along the Oz axis with velocity βc. The transverse force acting on the particle is

$$\mathbf{F}_\perp=e\{\boldsymbol{\mathcal{E}}_\perp+\beta[\mathbf{u}_3\boldsymbol{\mathcal{H}}_\perp]\}\,e^{i(\omega t-\varkappa z+\varphi_0)},\quad (4.26)$$

where φ_0—initial phase shift between the wave and the particle. We introduce the symbol $\beta_\varphi = v_\varphi/c = k/\kappa$ and use formulas (4.25), which take in this notation the form

$$\left.\begin{aligned}\varkappa(1-\beta_\varphi^2)\boldsymbol{\mathcal{E}}_\perp&=i\{\nabla_\perp\mathcal{E}_z-\beta_\varphi[\mathbf{u}_3\nabla_\perp\mathcal{H}_z]\},\\ \varkappa(1-\beta_\varphi^2)\boldsymbol{\mathcal{H}}_\perp&=i\{\nabla_\perp\mathcal{H}_z+\beta_\varphi[\mathbf{u}_3\nabla_\perp\mathcal{E}_z]\}.\end{aligned}\right\}\quad (4.27)$$

Substituting these expressions in (4.26) and expanding the double vector product, we get

$$\mathbf{F}_\perp=\frac{ie}{\varkappa}\left\{\frac{1-\beta_\varphi\beta}{1-\beta_\varphi^2}\nabla_\perp\mathcal{E}_z+\frac{\beta-\beta_\varphi}{1-\beta_\varphi^2}[\mathbf{u}_3\nabla_\perp\mathcal{H}_z]\right\}e^{i(\omega t-\varkappa z+\varphi_0)}.\quad (4.28)$$

This expression for the force is valid for an arbitrary particle velocity and for an arbitrary wave. For a particle moving with a velocity equal to the phase velocity of the wave ($\beta = \beta_\varphi$) and for $\varphi_0 = -\pi/2$, the second term in the curly brackets of (4.28) drops out

$$ie^{i(\omega t-\varkappa z+\varphi_0)}=1,$$

and the expression for the force assumes the very simple form

$$\mathbf{F}_\perp=\frac{e}{\varkappa}\nabla_\perp\mathcal{E}_z.\quad (4.29)$$

Waveguides for use as deflecting systems for separators must satisfy the same requirement as resonator systems, namely that the force must be the same for particles with different initial conditions entering the waveguide at the same instant of time. In addition, inasmuch as we are interested in separating particles of very high energy ($\beta \approx 1$), the electromagnetic wave must propagate with a phase velocity equal to the velocity of light. As is well known [53], when $v_\varphi = c$ the TE and TM modes become degenerate (the H_z or the E_z components are respectively equal to zero or constant), and do not propagate in the simplest waveguide structures. Thus, it becomes necessary to use a different mode, whose H_z and E_z components satisfy in accordance with (4.25) the following relations when $v_\varphi = c$:

$$\left.\begin{aligned}[\mathbf{u}_3\nabla_\perp\mathcal{H}_z]&=\nabla_\perp\mathcal{E}_z,\\ [\mathbf{u}_3\nabla_\perp\mathcal{E}_z]&=-\nabla_\perp\mathcal{H}_z.\end{aligned}\right\}\quad (4.30)$$

Since the field components of TE and TM waves vanish when $v_\varphi = c$, relations (4.3) are satisfied for them automatically. A theoretical investigation of the waves of the new type, propagating with phase velocity equal to the velocity of light, has been the subject of many works [52,55-57]. We present below an approximate derivation of the expressions for the field components of one such wave propagating in a cylindrical diaphragmed waveguide, and show that this wave corresponds fully to the conditions formulated above. The waveguide and the symbols are shown schematically in Fig. 14.

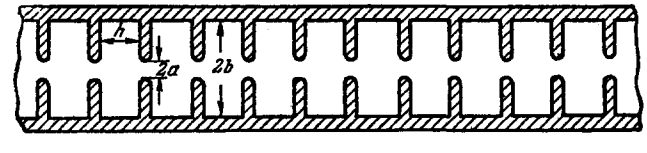

FIG. 14. Cylindrical diaphragmed waveguide.

The equations for the components of the electric field, obtained from Maxwell's equations (4.22), have in cylindrical coordinates the form

$$\left.\begin{aligned}\Delta\mathcal{E}_z+(k^2-\varkappa^2)\mathcal{E}_z&=0,\\ \Delta\mathcal{E}_r-\frac{1}{r^2}\left(\mathcal{E}_r+2\frac{\partial\mathcal{E}_\theta}{\partial\theta}\right)+(k^2-\varkappa^2)\mathcal{E}_r&=0,\\ \Delta\mathcal{E}_\theta-\frac{1}{r^2}\left(\mathcal{E}_\theta-2\frac{\partial\mathcal{E}_r}{\partial\theta}\right)+(k^2-\varkappa^2)\mathcal{E}_\theta&=0,\end{aligned}\right\}\quad (4.31)$$

where

$$\Delta = \frac{\partial^2}{\partial r^2} + \frac{1}{r}\frac{\partial}{\partial r} + \frac{1}{r^2}\frac{\partial^2}{\partial \theta^2}.$$

Determining $\partial \mathcal{E}_r/\partial\theta$ from Maxwell's equations $-ikH_z = (\text{curl } E)_z$, and $\partial \mathcal{E}_\theta/\partial\theta$ from the equation div E = 0, and substituting in (4.31), we obtain after simple transformations

$$\left.\begin{aligned} &\Delta \mathcal{E}_z + (k^2 - \varkappa^2)\mathcal{E}_z = 0,\\ &\frac{1}{r^2}\frac{\partial}{\partial r}\left(r\frac{\partial}{\partial r}(r\mathcal{E}_r)\right) + \frac{1}{r^2}\frac{\partial^2 \mathcal{E}_r}{\partial\theta^2} + (k^2-\varkappa^2)\mathcal{E}_r = \frac{2i\varkappa}{r}\mathcal{E}_z,\\ &\frac{1}{r^2}\frac{\partial}{\partial r}\left(r\frac{\partial}{\partial r}(r\mathcal{E}_\theta)\right) + \frac{1}{r^2}\frac{\partial^2 \mathcal{E}_\theta}{\partial\theta^2} + (k^2-\varkappa^2)\mathcal{E}_\theta = -\frac{2ik}{r}\mathcal{H}_z. \end{aligned}\right\} \quad (4.32)$$

Analogously we obtain equations for the components of the magnetic field:

$$\left.\begin{aligned} &\Delta \mathcal{H}_z + (k^2 - \varkappa^2)\mathcal{H}_z = 0,\\ &\frac{1}{r^2}\frac{\partial}{\partial r}\left(r\frac{\partial}{\partial r}(r\mathcal{H}_r)\right) + \frac{1}{r^2}\frac{\partial^2 \mathcal{H}_r}{\partial\theta^2} + (k^2-\varkappa^2)\mathcal{H}_r = \frac{2i\varkappa}{r}\mathcal{H}_z,\\ &\frac{1}{r^2}\frac{\partial}{\partial r}\left(r\frac{\partial}{\partial r}(r\mathcal{H}_\theta)\right) + \frac{1}{r^2}\frac{\partial^2 \mathcal{H}_\theta}{\partial\theta^2} + (k^2-\varkappa^2)\mathcal{H}_\theta = \frac{2ik}{r}\mathcal{E}_z. \end{aligned}\right\} \quad (4.33)$$

When the phase velocity is equal to the velocity of light, $k^2 = \kappa^2$, the last term in the left half of (4.32) and (4.33) drops out. In addition, we put $\mathcal{E} = P(r)e^{in\theta}$ and $\mathcal{H} = G(r)e^{in\theta}$, and consider the expressions for the components of the field of the fundamental wave with n = 1. Allowing for all these factors, Eqs. (4.32) and (4.33) take the form

$$\left.\begin{aligned} &\frac{d^2P_z}{dr^2} + \frac{1}{r}\frac{dP_z}{dr} - \frac{P_z}{r^2} = 0, \qquad \frac{d^2G_z}{dr^2} + \frac{1}{r}\frac{dG_z}{dr} - \frac{G_z}{r^2} = 0,\\ &\frac{d^2P_r}{dr^2} + \frac{3}{r}\frac{dP_r}{dr} = \frac{2ik}{r}P_z, \qquad \frac{d^2G_r}{dr^2} + \frac{3}{r}\frac{dG_r}{dr} = \frac{2ik}{r}G_z,\\ &\frac{d^2P_\theta}{dr^2} + \frac{3}{r}\frac{dP_\theta}{dr} = -\frac{2ik}{r}G_z, \qquad \frac{d^2G_\theta}{dr^2} + \frac{3}{r}\frac{dG_\theta}{dr} = \frac{2ik}{r}P_z. \end{aligned}\right\} \quad (4.34)$$

The solutions of these equations in the propagation region, under the conditions that they be bounded at r = 0, are determined by the following formulas:

$$\left.\begin{aligned} &P_z = Dkr, \qquad G_z = iDkr,\\ &P_r = -i\left[M - D\left(\frac{kr}{2}\right)^2\right], \qquad G_r = -\left[M + D + D\left(\frac{kr}{2}\right)^2\right],\\ &P_\theta = M + D\left(\frac{kr}{2}\right)^2, \qquad G_\theta = i\left[-M - D + D\left(\frac{kr}{2}\right)^2\right], \end{aligned}\right\} \quad (4.35)$$

where M and D are constants determined from the boundary conditions for r = a. Since the solutions in the space between the diaphragms are of no interest to us, they are not written out here. Moreover, in the first approximation, which is perfectly adequate for our purposes, these expressions will not be needed at all, as will be shown below. We assume that the wavelength is much longer than the period of the waveguide structure, i.e., $\lambda \gg h$, where h is the distance between diaphragms. Since the E_θ field component should vanish on the surfaces of the diaphragms, we can in first approximation assume for $\lambda \gg h$ that $E_\theta = 0$ everywhere at r = a. From this condition we determine the constant M:

$$M = -D\left(\frac{ka}{2}\right)^2. \quad (4.36)$$

Taking (4.36) and (4.35) into account, as well as the equations div E = 0 and div H = 0, we obtain for the field components the following final expressions:

$$\left.\begin{aligned} &E_z = Dkr\begin{matrix}\cos\theta\\ \sin\theta\end{matrix} e^{i(\omega t - kz)},\\ &E_r = iD\left[\left(\frac{kr}{2}\right)^2 + \left(\frac{ka}{2}\right)^2\right]\begin{matrix}\cos\theta\\ \sin\theta\end{matrix} e^{i(\omega t - kz)},\\ &E_\theta = iD\left[\left(\frac{kr}{2}\right)^2 - \left(\frac{ka}{2}\right)^2\right]\begin{matrix}\sin\theta\\ -\cos\theta\end{matrix} e^{i(\omega t - kz)},\\ &H_z = -Dkr\begin{matrix}\sin\theta\\ \cos\theta\end{matrix} e^{i(\omega t - kz)},\\ &H_r = -iD\left[\left(\frac{kr}{2}\right)^2 - \left(\frac{ka}{2}\right)^2 + 1\right]\begin{matrix}\sin\theta\\ \cos\theta\end{matrix} e^{i(\omega t - kz)},\\ &H_\theta = iD\left[\left(\frac{kr}{2}\right)^2 + \left(\frac{ka}{2}\right)^2 - 1\right]\begin{matrix}\cos\theta\\ -\sin\theta\end{matrix} e^{i(\omega t - kz)}. \end{aligned}\right\} \quad (4.37)$$

If we choose in (4.37) the first form of the dependence of E and H on θ ($E_Z = D\,kr\cos\theta\exp[i(\omega - hz)]$ etc.) and go from cylindrical to rectangular coordinates ($x = r\cos\theta$, $y = r\sin\theta$) then, taking (4.29) into account, we find that the force acting on the particle is constant in magnitude and in direction in the entire structure:

$$\left.\begin{aligned} F_x &= eD,\\ F_y &= 0. \end{aligned}\right\} \quad (4.38)$$

For the other dependence of E and H on θ we obtain, to the contrary, $F_X = 0$ and $F_Y = eD$. This remarkable feature of the described high-frequency structure has been attracting the interest of physicists, and such waveguides have been thoroughly investigated not only theoretically but also experimentally [58-60]. In this connection we present a few energy relations of practical use [60]. We assume that the wave excited in the waveguide is such that the particle acquires a transverse deflection only in the x direction. Then, according to (4.29), the transverse momentum acquired by the particle on passing through a waveguide of length l will be given by

$$p_\perp = \frac{e}{\omega}\int_0^l \frac{\partial E_z}{\partial x}\,dz. \quad (4.39)$$

We introduce the concept of shunt impedance (the ratio of the square of the energy per unit length to the loss power)

$$R = \frac{\left\langle\left(\frac{1}{k}\frac{\partial E_z}{\partial x}\right)^2\right\rangle}{-\frac{d\langle\mathcal{P}\rangle}{dz}}, \quad (4.40)$$

where $\mathcal{P}$—power flux in the structure and the symbol $\langle\,\rangle$ denotes time averaging.

It is natural to assume that $\langle\mathcal{P}\rangle$ varies along the waveguide axis in accordance with

$$\langle\mathcal{P}\rangle = \mathcal{P}_0 e^{-2Iz}, \quad (4.41)$$

where 2I is the attenuation factor.

Using (4.40) and (4.41) we can rewrite (4.39) in the form

$$p_\perp = \frac{ek}{\omega}\sqrt{2IR\mathcal{P}_0}\left(\frac{1-e^{-Il}}{I}\right). \qquad (4.42)$$

We see therefore that the optimal value of $p_\perp$ can be obtained by choosing the corresponding values of the parameters R, I, and l. We express the shunt resistance R in terms of the characteristics of the waveguide. To this end we make use of the expression for the fields (4.37) and integrate the Umov-Poynting vector over the cross section bounded by the aperture of the diaphragm. We then obtain for the power flux in the z direction

$$\langle \mathcal{P}_z \rangle = \frac{D^2a^2c}{8}\left(\frac{ka}{2}\right)^2\left[\frac{4}{3}\left(\frac{ka}{2}\right)^2 - 1\right]. \qquad (4.43)$$

From this it follows, in particular, that the sign of $\langle \mathcal{P} \rangle$ will depend on whether $ka > \sqrt{3}$ or $ka < \sqrt{3}$. Physically this means none other than the presence of opposite signs of the group velocity v_{gr} relative to the wave propagation direction. Noting that

$$I = \frac{\omega}{2v_{gr}Q},$$

where Q is the figure of merit of the waveguide in the resonant mode; using (4.37) and (4.43), we obtain ultimately from (4.40)

$$R = \frac{4v_{gr}Q}{\omega c a^2\left(\frac{ka}{2}\right)^2\left[\frac{4}{3}\left(\frac{ka}{2}\right)^2 - 1\right]}. \qquad (4.44)$$

Unfortunately, at the present time there is no analytic expression for v_{gr} in terms of the characteristic structure, and the latter must be measured experimentally.[60]

3. High Frequency Separator for the Two-Mile Stanford Linear Electron Accelerator

A linear electron accelerator with energy up to 40 GeV is now being built at Stanford. In this connection, a high frequency separator is under development and different models for it are under study [60]. Since the beam at the exit from the accelerator will be in the form of clusters that follow each other periodically with a frequency of 2856 Mcs ($\lambda \simeq 10.5$ cm) and with a high off-duty factor (60—70), it is most advantageous to employ the separator proposed by Panofsky, the operating principle of which was considered in Sec. 1 of the present chapter. The operating frequency of the Stanford separator was chosen to coincide with the operating frequency of the accelerator. The deflector proposed is a section of a diaphragmed cylindrical waveguide whose high-frequency field configuration was calculated in detail in Sec. 2 of this chapter.

Let us stop to discuss the results of the cold measurements of the section of the diaphragmed waveguide in one of the models of the high frequency separator [60]. The configuration of the electric field in such a structure (Fig. 15) is determined by the small-perturbation method, using a sapphire disc as a probe. Figures 16 and 17 show the results of measurements of the frequency shift $\Delta f \sim E^2$, obtained by moving the disc along the axis and along the radius of the waveguide. The same figures show the dimensions of the probe and of all the waveguide elements. It is most advantageous to employ this high frequency deflector to operate in the traveling-wave mode.

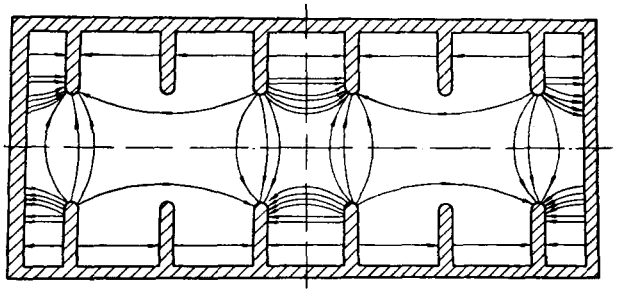

FIG. 15. Field configuration in a section of a cylindrical diaphragmed waveguide.

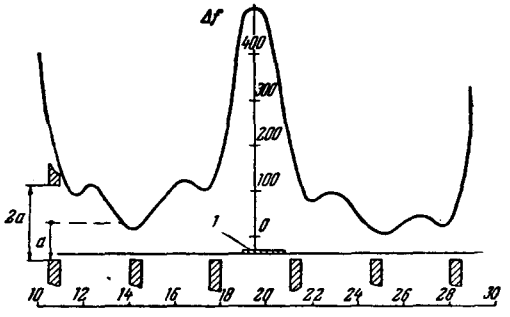

FIG. 16. Dependence of the frequency shift $\Delta f \sim E^2$ along the axis of a cylindrical diaphragmed waveguide. 1—Sapphire probe.

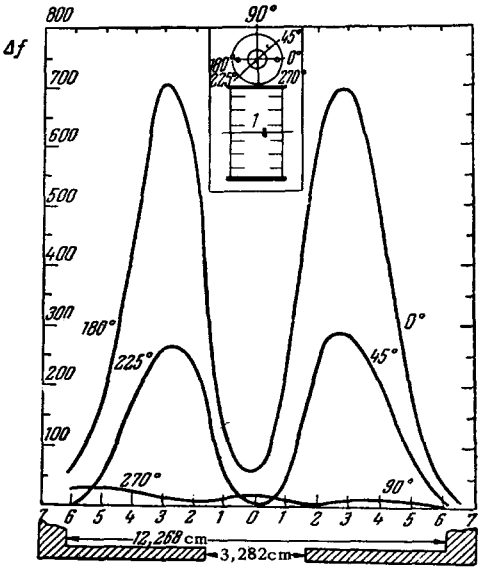

FIG. 17. Dependence of the frequency shift $\Delta f \sim E^2$ along the radius of the waveguide. 1—Sapphire probe (the apertures in the diaphragms are intended to maintain the polarization plane of the wave).

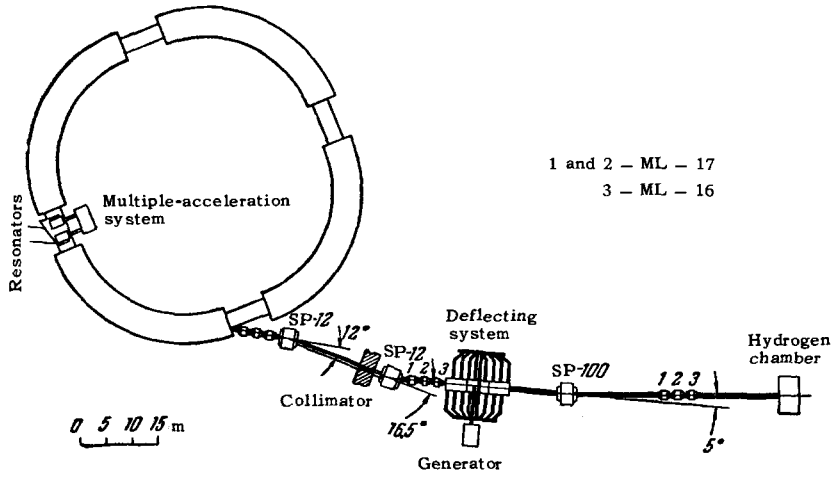

FIG. 18. Diagram of electrodynamic particle separator of the Joint Institute for Nuclear Research.

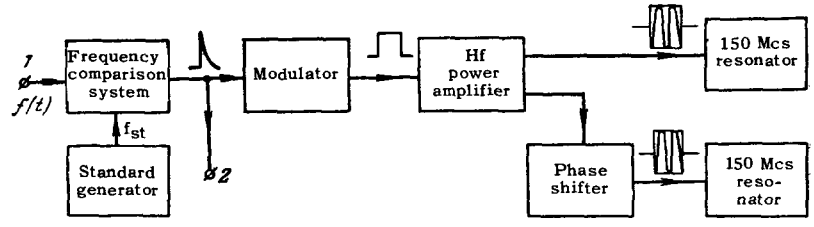

FIG. 19. Block diagram of multiple acceleration system of the electrodynamic separator of the Joint Institute for Nuclear Research. 1. Accelerating frequency of the Joint Institute proton synchrotron; 2–pulse that switches the accelerating voltage off.

Depending on the choice of the waveguide parameters, we can obtain a corresponding phase shift ψ per cell, and also the value and sign of the group velocity v_{gr}. For the model presented $\psi = 2\pi/3$ and $v_{gr} = -0.0296$ c.*

4. Electrodynamic Particle Separator of the Joint Institute for Nuclear Research

At the present time the high-energy laboratory of the Joint Institute for Nuclear Research has completed the development of an electrodynamic particle separator [62] based on the separation principle proposed by V. I. Veksler and V. A. Petukhov and described above. The electrodynamic separator is based on the following: a system for multiple acceleration and a system for extraction of a secondary-particle beam from the accelerator, a deflecting unit, and an ion-optical system. A diagram of the channel is shown in Fig. 18.

a) Multiple acceleration system and system for extraction of the separated beam from the accelerator. The purpose of the multiple acceleration system is to obtain the high-frequency beam structure necessary for the separation. This is attained by intercepting the protons accelerated in the proton synchrotron from the ordinary acceleration mode into the multiple acceleration mode [63]. The transition to multiple acceleration takes place at the end of the acceleration cycle, when the protons have their required energy. The chosen operating frequency of the multiple-acceleration system is 150 Mc and the corresponding multiplicity is $q \simeq 100$. To ensure an interception coefficient $\sigma > 0.5$ with such a multiplicity, the accelerating voltage V_q must be 250 kV. The accuracy with which the proton synchrotron acceleration system is switched off and the multiple acceleration system switches on should be within 10^{-4} (in terms of frequency).

Figure 19 shows a block diagram of the multiple acceleration system. The accelerating voltage is produced by two resonators, which are installed in the vacuum chamber of the accelerator in one of its straight-line sections. Each resonator is a quarter-wave coaxial line segment. The need for enclosing the resonator in the vacuum chamber makes its shunt resistance relatively low, ~40 kilohms.

To obtain a voltage on the order of 125 kV on the accelerating slot, the power required is on the order of 100 kW. The resonators are fed from a four-stage separately-excited generator with two parallel outputs. The specified accuracy with which the frequency is to be maintained is ensured by a quartz exciter which is common to the multiple-acceleration system and the deflection unit. These two devices are rigidly coupled in phase. The multiple-acceleration system is designed for pulsed operation in each acceleration cycle, with a duration not more than 20 milliseconds.

The secondary particles produced by the interaction between the accelerated beam and the target are

*Analogous waveguides were investigated in many other laboratories. Thus, for example, waveguides with $\psi = \pi/2$ and $v_{gr} = 0.0903c$ are investigated at CERN [61], and with $\psi = \pi/2$ $v_{gr} < 0$ in Brookhaven [60].

extracted by inducing for a short time azimuthal asymmetry of the magnetic field of the proton synchrotron [64]. This makes it possible to extract the particles within less than 5 milliseconds, retaining at the same time the specified high frequency structure.

b) Deflecting unit. The parameters of the deflecting unit are chosen for separation of 5 GeV/c antiprotons and pions. The center of the deflection unit is 59 meters distant from the target. It is possible in this case to separate also antiprotons and pions with smaller momenta (2.9 and 2.2 GeV/c).

The deflecting unit [54] is constructed in the form of a system of 16 independently phased quasitoroidal resonators (Fig. 20). The resonators operate at the fundamental mode and a high-frequency electric field is used for the particle deflection. As was already noted in Sec. 2, such a resonator form ensures the passage of the separated particles predominantly through the resonator region where the electric field is concentrated. In view of the considerable resonator aperture sizes necessary for the passage of the beam, measures are taken to eliminate coupling between the resonators. Suppression of the high frequency resonant discharge is provided in the construction of the resonator. The setting of the resonator frequency and accordingly the maintenance of the specified phase is by means of frequency-phase adjustment systems.

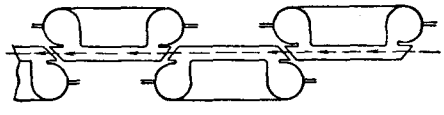

FIG. 20. Arrangement of the resonators of the deflecting unit of the Joint Institute electrodynamic separator.

The deflecting unit is fed from a five-stage generator with separate excitation and 1500 kW available power. The generator makes possible pulsed operation of the deflecting unit at 6 pulses per minute, with 6 millisecond pulses.

The generator power distribution system is constructed on the principle of combining a two-step power-branching "tree" with subsequent direct power branching in the resonator groups. Each group consists of four resonators connected in parallel by means of half-wave feeder segments.

The required phase relations between the resonators is established with the aid of matched phase shifters of the trombone type. Figure 21 shows the over-all view of the deflecting unit of the electrodynamic separator of the High Energy Laboratory of the Joint Institute for Nuclear Research.

The main parameters of the deflecting unit are as follows: operating frequency f = 150 Mcs, length of deflecting unit l = 12 meters, number of resonators n = 16, shunt resistance of the resonator $R_{sh} \geq 0.8$ megohm. At an electric field intensity ~ 30 kV/cm, the power losses in each resonator amount to ~ 60 kW. The angle divergence of the 5 GeV/c pions and antiprotons passing through the deflecting unit is approximately 8 mrad.

c) Ion-optical system. The ion-optical system consists of three objectives (see Fig. 18), each comprising a triplet of three standard ML-17 and ML-16 lenses (see [71]). The first objective produces a parallel beam of particles emitted from the target. The target is in the magnetic field of the proton synchrotron. Its position is calculated to cause the particles produced in the target at an angle of 0° to pass in the specified direction. The second objective focuses the beam on the entrance to a

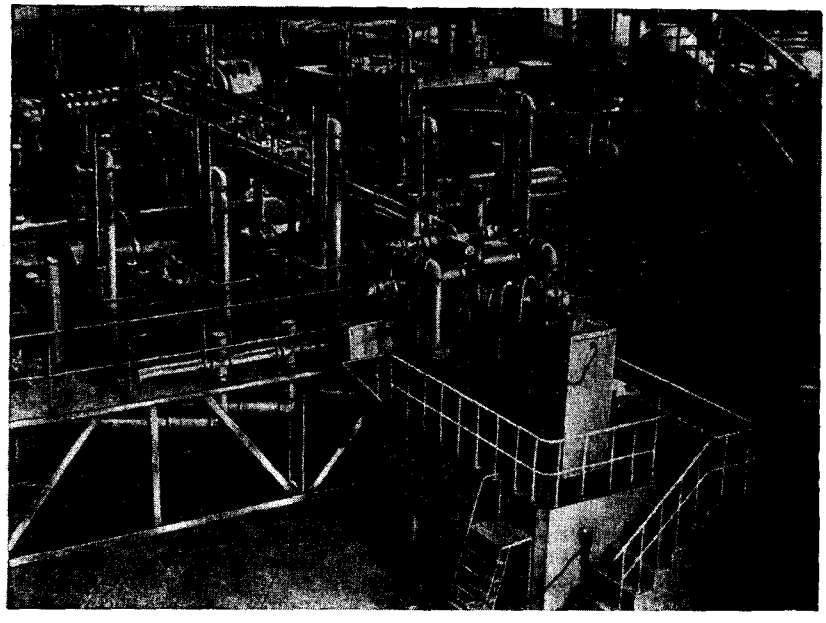

FIG. 21. Over-all view of the deflecting unit of the Joint Institute electrodynamic separator.

special dual magnet SP-100. The construction of the magnet is such that the separated particles (say pions and antiprotons) move through it in magnetic fields of opposite directions, and consequently acquire opposite angular deflections. This deflection is approximately 10 times larger than the angular deflection imparted by the deflecting unit to the particles. Finally, the third objective focuses the beam on the hydrogen bubble chamber, which is located at the end of the channel.

Electromagnets SP-12 are used to separate the required momentum interval and for subsequent compensation for the dispersion produced in the momentum analysis. The particles move on the entire path from the accelerator to the hydrogen chamber in an ion duct in which a vacuum of 10^{-3} mm Hg is maintained. The high vacuum in the deflecting unit (10^{-6} mm Hg) is separated from the lower vacuum in the ion duct by 10 mylar partitions.

Table III summarizes the main characteristics of the electrodynamic separator.

Table III. Principal characteristics of electrodynamic separator

Particle momentum	5 GeV/c
Momentum interval $\left(\frac{\Delta p}{p}\right)$ . . .	0.02
Expected antiproton intensity	$1\tilde{p}/10^{10}p$
Expected separation coefficient	10^3
Channel length	115 m
Working wavelength	2 m
Acceleration multiplicity	100
High frequency pulse power:	
a) system for multiple acceleration	0.3 MW
b) deflecting unit	1.0 MW

5. CERN High-Frequency Separator

The ideas of electrodynamic mass separation of particles, developed in recent years at CERN, are reflected in the design of a special channel for pure beams of K-mesons, pions, protons, and antiprotons with particle momenta up to 15 GeV/c.[65] This channel is intended for the 1-1/2 meter British liquid-hydrogen chamber. A feature of the channel (Fig. 22) is that it is designed to operate with either electrostatic ordinary deflectors or with high frequency deflectors. In the latter case it is proposed to effect the separation first with the aid of two high frequency deflectors and later with three deflectors.

a) Ion-optical system of the channel. The use of several targets is proposed to obtain intense beams of secondary particles with different momenta. All the targets should extract the beam at zero or near-zero particle-production angles. The ion-optical system will consist of standard electromagnets and CERN magnetic quadrupole lenses. When working with electrostatic separators, the ion-optical system of the channel is optimized to produce a K-meson beam with momenta up to 5 GeV/c. When working in the dynamic separation mode, the ion-optical system is optimized to produce 10-GeV/c K mesons. Let us discuss in greater detail the electrodynamic separation of particles. As in the case of the electrostatic separation of the beam, the channel can be divided in three parts: the first part determines the acceptance of the system and the momentum interval of the separated particles. It consists of vertical and horizontal collimators K_1 and K_2, respectively, which set the acceptance in two planes, and a triplet of quadrupole lenses Q_1, Q_2, and Q_3. These lenses focus the beam onto the centers of the collimators K_3 and K_4 in the horizontal and vertical planes, respectively. Turning magnets M_1 and M_2 produce dispersion of the horizontal image in K_3, thereby ensuring separation of the required momentum interval at this point. The horizontal and vertical images are separated in order to reduce the background due to muons and scattered particles.

The beam passing through the lens doublet Q_4 and turning magnets M_3 and M_4 has no dispersion, because it is turned by each of the magnets by the same amount and because the centers of the magnets M_1, M_2, M_3, and M_4 are conjugate foci of the lens doublet Q_3 and Q_4. The collimator K_4 is the source for the first beam mass separation stage when operating with the electrostatic deflectors. A horizontal and vertical image are produced in the first deflector by the lens quadrupole Q_4, Q_5, Q_6, and Q_7, and in the second deflector by Q_8, Q_9, Q_{10}, and Q_{11}.

The vertical collimator K_5 is an angle slot and serves as the source for the separating stage when using the high-frequency deflectors.

The mass separation of the particles occurs in an absorber placed on the beam axis. The image of the slot K_5 is focused on the absorber. The subsequent part of the channel forms the beam directly for the bubble chamber.

b) Deflecting system. The deflector of the deflecting system is a large homogeneous diaphragmed

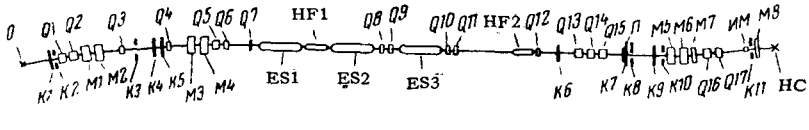

FIG. 22. Diagram of CERN channel for production of pure beams, using electrostatic and high-frequency separation. The electrostatic deflectors are designated ES, the high-frequency ones HF.

waveguide operating in the traveling-wave mode. The length of each deflector is 3 meters. The construction of the waveguide is the same as in an electron linear accelerator, but the types of electromagnetic fields analyzed in detail in Sec. 2 are employed.

A feature of the deflecting system is that it can operate periodically, in short pulses. The duration of such pulses does not exceed several microseconds. This imposes, in particular, definite requirements on the extraction of the particles from the accelerator.

The technology developed at CERN for the manufacture of waveguides makes it possible to produce them in lengths up to 1 meter. Each deflector must be pumped out during operation to a pressure on the order of 10^{-6} mm Hg. It is assumed that the deflectors will be separated from the individual sections of the channel with lower vacuum with the aid of six-micron mylar windows.

The main parameters of the CERN separator are listed in Table IV.

Table IV. Main parameters of the separator

Nominal frequency (λ_0 = 10.5 cm)	2856 Mc
Calculated momentum (K-meson separation)	10.34 GeV/c
Calculated momentum (antiproton separation)	20.24 GeV/c
Distance between deflectors	50 m
Deflector length	3 m
Deflector aperture	54 mm
Maximum transverse momentum imparted to the particles in the deflector	20 MeV/c
Maximum high-frequency power in deflector	17 MW

6. Field of Application and Propects of Development of High-frequency Separators

Development of high frequency separation methods started relatively recently and is not as yet at the same state of perfection as, for example, of the electrostatic method. We can therefore not indicate a definite region of application of the high frequency separators. It is interesting to compare this method with the electrostatic one [61].

In electrostatic separators the particle-separation angle, in the relativistic approximation, is equal to [see (3.7)]

$$\Delta\alpha_e = \frac{e\mathcal{E}l\,(E_{02}^2 - E_{01}^2)}{2\,(pc)^3}. \qquad (4.45)$$

The angle for high frequency separators can be represented in the form [see (4.3)]

$$\Delta\alpha_g = \frac{2e\delta l}{pc}. \qquad (4.46)$$

In this case the following condition should be satisfied [see (4.5)]

$$\frac{L}{\lambda}\,\frac{E_{02}^2 - E_{01}^2}{(pc)^2} = 1, \qquad (4.47)$$

the meaning of which, as already indicated, is that particles of different species acquire at the end of the travel base L under identical initial conditions a phase difference equal to π. Combining (4.46) and (4.47) we obtain

$$\Delta\alpha_g = \frac{e\mathcal{E}l\,(E_{02}^2 - E_{01}^2)}{2\,(pc)^3}\,\frac{4L}{\lambda}. \qquad (4.48)$$

Comparison of (4.45) and (4.48) shows the main advantage of the high-frequency separation method over the electrostatic method. Indeed, as follows from (4.45) and (4.48), for identical momenta, field intensities, and deflector lengths* the obtained separation angle $\Delta\alpha_g$ is $4L/\lambda$ times larger than the angle $\Delta\alpha_e$. This gain is due to the fact that for electrostatic separation the difference in the transverse momenta acquired by particles of unequal mass passing through the deflector is proportional to the difference in the time of flight. For the high-frequency method this difference is simply proportional to the time of flight through the deflector itself. As a result the separation angle $\Delta\alpha_e$ is inversely proportional to the cube of the momentum [see (4.45)], whereas $\Delta\alpha_g$ is inversely proportional to the momentum [see (4.46)]. When centimeter wavelengths are used with a flight base of several hundred meters, the factor $4L/\lambda$ reaches 10^4 and more. It therefore becomes possible to advance in energy by more than one order of magnitude compared with the electrostatic method. Thus, for example, in the CERN 100-GeV high-frequency separator [66,67] now planned in connection with the design of a large proton synchrotron for 150—300 GeV, it is proposed to employ a wavelength λ = 3 cm and a flight base L of more than 1,000 meters. Of course, this raises many serious problems. One is the phasing of high-frequency deflectors that are separated by several tens of thousands of wavelengths. Another is the duration of the high frequency pulse. The existing high frequency power sources in the centimeter band yield large pulsed power (tens of megawatts) only for durations not exceeding several microseconds. However, in future large cyclic accelerators for ultrarelativistic energies, even the fastest (single-turn) extraction of the particles to the target will last several dozen microseconds. This means that it is possible to use effectively only a portion of the accelerated beam. It is therefore extremely desirable to increase the

*In fact, the length of the high-frequency deflectors in the separators now under design or construction (l = 2 – 3 meters) is approximately one order of magnitude smaller than the lengths of the electrostatic deflectors (l = 20 meters). This, however, does not affect the reasoning.

duration of the high frequency pulses. A similar requirement, but even more stringent, arises when an attempt is made to use spark chambers and Cerenkov counters for investigations in pure beams. One possible way of increasing the duration is to use high-frequency superconducting deflecting devices [68]. Superconducting resonators have very high Q, for example, the measured Q of a resonator for the 10 cm band is 3,000 times larger at 1.8° K than at room temperature, reaching 3×10^8 [69]. In addition, allowance should be made for the fact that the loading of the high frequency deflectors by the beam in the separator is negligibly small, owing to the exceptionally weak intensity of the beam. All this favors the use of superconducting high frequency structures for particle separation. Calculations show that in order for the particles to acquire a transverse momentum on the order of 20 MeV/c it is necessary to have in this case not 15 megawatts but only 5 kilowatts. At such a power level, the centimeter-band generators (klystrons) can operate almost continuously. The question of the behavior of superconductors in strong high frequency fields is not clear as yet, but similar research is being carried out in many laboratories [68].

CONCLUSION

We have considered the principal methods of particle separation. As can be seen from the appended bibliography, this is a relatively recent trend in high-energy physics. However, even at present a pure-beam channel is an essential part of any high-power accelerator. The most widely used for the time being are electrostatic separators, used to produce pure beams with energies of several GeV. The problem of particle separation at energies of tens and perhaps hundreds of GeV can be solved with electrodynamic separators, which are under intense development in many laboratories.

Progress in elementary-particle physics calls for having more and more accelerated-particle energies. Accelerators are already being designed for 200—1,000 GeV. The question of the identification of particles of such energies has not yet been solved. New methods for the creation of pure beams of ultrarelativistic particles will be necessary. In this connection, attention should be paid to the suggestion that particles be separated on the basis of the differences in such characteristics of their nuclear interactions as total cross sections, kinematics, and angular distributions [70]. For the time being it is still difficult to judge the practical value of this suggestion. It is clear, however, that as accelerators for ultrarelativistic energies become available new ways of particle separation will also be found.

[1] H. K. Ticho, The Production, Transport and Separation of Beams, Proceedings of International Conference on High Energy Accelerators and Instrumentation, CERN, 1959, p. 387.

[2] R. L. Cool, Particle Production by High Energy Accelerators, Proceedings of International Conference on High Energy Accelerators, Brookhaven, 1961, p. 15.

[3] B. Rossi, High Energy Particles (Russian translation), Gostekhizdat, 1955, p. 49 [Printice Hall, New York, 1952].

[4] G. Goldhaber and S. Goldhaber, CERN, Internal Report, 60—13, 1960.

[5] Meyer, Perl, and Glaser, A Scattering of K^+ Mesons or Protons. Phys. Rev. 107, 279 (1957).

[6] S. Marcowitz and L. Ratnen, Separation Scheme for High Energy Particles by Differential Energy Loss and Momentum Analysis, Rev. Sci. Instr. 5, 552 (1962).

[7] Baldin, Gol'danskiĭ, and Rozental', Kinematika yadernykh reaktsiĭ (Kinematics of Nuclear Reactions), Fizmatgiz, 1959.

[8] A. Citron and H. Overas, On a Focusing Channel for Collecting μ Mesons from $\pi \rightarrow \mu$ Decay in Flight, CERN/SC 143, 1957.

[9] Braunersrenther, Chaband, Delorme, and Morpurgo, Lentilles quadrupolaires magnetiques constituant le dispositif de focalisation du faisceau de mesons μ du CERN, CERN 61—62, 1961.

[10] Abrosimov, Kaminker, Petrov, and Sherman. Contribution to the Theory of a Channel Made up of Quadrupole-Lense Magnets to Obtain Pure Muon Beams. Transactions, International Conference on Charged-particle Accelerators, Dubna, 1963 (in press). ZhTF 34, 313 (1964), Soviet Phys. Tech. Phys.

[11] N. A. Burgov, and A. G. Beda, Shaping of a High-Energy Muon Beam. Transactions, International Conference on Charged-Particle Acceleration, Dubna, 1963 (in press).

[12] Citron, Delorme, Farley, Goldzahl, Heintze, Michaelis, Morpurgo, and Overas, A High-intensity μ Meson Beam from the 600 Mev CERN Synchrocyclotron, Proceedings of International Conference on Instrumentation for High-energy Physics, Berkeley, California,1960, p. 286.

[13] T. D. Lee and C. N. Yang, Theoretical Discussions on Possible High-energy Neutrino Experiments, Phys. Rev. Letts. 4, 307 (1960).

[14] Griesch, Kuiper, Langeseth, van der Meer, Neet, Plass, Pluym, and de Raad, Status of Magnetic Horn and Neutrino Beam, Nucl. Instr. and Meth. 20, 58 (1963).

[15] S. Van der Meer, A Directive Device for Charged Particles and its Use in an Enhanced Neutrino Beam, CERN 61—7, 1961.

[16] Bingham, Burmeister, Cundy, Innocenti, Lecaurtois, Mollerud, Myatt, Paty, Perkins, Ramm, Schultze, Sletter, Soop, Voss, and Yoshiki, Neutrino experiment-bubble chamber results, International

Conference on Elementary Particles, Sienna, Italy, 1963.

[17] C. Germain, Principe du separateur electrostatique, CERN, 59—30, 1959.

[18] Coombes, Cork, Galbraith, Lambertson, Wenzel, Antiproton-proton Cross Sections at 133, 197 and 333 Mev, Phys. Rev. 112, 1303, 1958.

[19] Berley, Duboc, Duong, Eberhard, George, Henri, Poyen, Allard, Bohy, Boldt, Tauneau, Kayas, Morellet, and Wagyelsy, Faisceau separé de mésons K^+ de 0.7 á 1.7 GeV/c, Nucl. Instr. and Meth. 24, 133 (1963).

[20] Eberhard, Good, and Ticho, Separated 1.17 BeV/c K^- Meson beam, Rev. Sci. Inst. 31, 1054 (1060).

[21] E. D. Courant, and R. Cool, Transport and Separation of Beams from AG Synchrotron, International Conference on High-energy Accelerators and Instrumentation, CERN, 1959, 403.

[22] E. D. Courant and L. Marshall, Mass Separation of Particles, Rev. Sci. Inst. 31, 193 (1960).

[23] S. van der Meer, Achromatic Beam Optics for Particle Separator, CERN 60—22, 1960.

[24] Baltay, Fowler, Sanford, Sandweiss, Brown, Fowler, and Webster, Design and Performance of a 3.3 BeV/c Separated Antiproton Beam, Energy Accelerators, Brookhaven, 1961, p. 452.

[25] C. Germain and R. Tinguely, Electrostatic Separator Technique at CERN, Nucl. Instr. Meth. 20, 21 (1963).

[26] Baltay, Sandweiss, Sandford, Brown, Webster and S. Yamamoto, The Separated Beam at the AGS Performance with Antiprotons and π^+ Mesons, Nucl. Instr. Meth. 20, 38 (1963).

[27] Leither, Moneti, and Samios, Performance of the AGS Separated Beam with High-energy Kaons, Nucl. Instr. Meth. 20, 42 (1963).

[28] Amoto, Courant, Filthuth, Malamud, Petrucei, Segar, Toner and Willis, A One-stage Separated K Meson Beam of 1.5 GeV/c Momentum at the CPS, Nucl. Inst. Meth. 20, 47 (1963).

[29] Aubert, Courant, Filthuth, Segar, and Willis, Low Energy Separated Beam at the CERN PS, Nucl. Inst. and Meth. 20, 51 (1963).

[30] J. J. Goldberg and J. M. Perreau, An faisceau d'usage general a deux etages de separation electrostatique an P. S., CERN 63—12, 1963.

[31] E. Keil and W. W. Neale, A High Momentum Separated Particle Beam for Use with the 1.5 Metre British National Hydrogen Bubble Chamber at CERN, Op. cit. [11].

[32] Good, Hillis, Lyman, and Terandy, Particle Separators at Argonne National Laboratory, Op. cit [11].

[33] M. L. Good, Electromagnetic Mass Separation at High-Energy, Proceedings of an International Conference on Instrumentation for High-energy Physics, CERN, 1960, p. 34.

[34] C. Germain, Extension of the Use of Electrostatic Separators in High Energies, Op. cit. [11].

[35] J. J. Murray, Glass Cathodes in Vacuum-insulated High-voltage systems, Proceedings of International Conference on Instrumentation for High-Energy physics, CERN, 1960, p. 25.

[36] W. K. H. Panofsky, A Mass Sensitive Deflector for High energy Particles HEPL (Internal memo) High-Energy Physics Laboratory, Stanford University, Stanford, California (May, 1956).

[37] D. V. Volkov, Possibility of Mass Separation of Relativistic Particles With the Aid of Waveguides with Traveling-Wave, ZhTF 3, 414 (1959).

[38] V. I. Veksler, Starting of Proton Synchrotron for 10 BeV and First Result of Physical Investigations. Transactions, Second International Geneva Conference, 1958. Papers of Soviet Scientists, Nuclear Physics, Atomizdat, Moscow, 1959, p. 253.

[39] Zubarev, Kladnitskiĭ, Kuznetsov, Mukhin, Okhrimenko, Rubin, and Semenyushkin. Physical Principles of Antiproton Channel. Preprint, Joint Institute for Nuclear Research, R-371, Dubna, 1959.

[40] J. P. Blewett, R. F. Separator of Mass for Complete Separation of High Energy Particle Beams, Proceedings International Conference on High Energy Accelerators and Instrumentation, CERN, 1959, p. 422.

[41] W. K. H. Panofsky, Remarks on High Energy Microwave Separators, CERN, Geneva, Switzerland, 1959 (Internal Memorandum).

[42] W. Schnell, Discussion of Radio Frequency Particle Separator for the CERN Proton Synchrotron, CERN, Report No. 61—5, CERN, Geneva, Switzerland.

[43] M. Geiger, Particle Separation by Means of a Chain of rf Deflection Cavities, Part I—II, CERN, PS/Int. AR/Psep, 60—4, CERN, Geneva, Switzerland.

[44] M. Geiger, Some Considerations on Particle Separation by Means of rf Deflection Using Cavities, CERN, Report No AR/60—13, CERN, Geneva, Switzerland.

[45] P. Lapostolle, Sur la déflection d'une particule rapide par un champ électromagnétique, CERN PS/Int. AR/PSep, 60—2, CERN, Geneva, Switzerland.

[46] P. Lapostolle, Focalisation alternée dans un séparateur haute fréquence; séparateurs parametriques, CERN PS/Int. AR/PSep. 60—5, CERN, Geneva, Switzerland.

[47] P. Lapostolle, Quelques relations approximatives concernant la séparation de particules de même quantité de mouvement mais de masse differente au moyen de champs de haute fréquence, CERN PS/Int. AR/60—15, CERN, Geneva, Switzerland.

[48] B. W. Montague and R. F. Travelling, Wave Particle Separators: a Matrix Formalism and General Phase Space Properties, CERN PS/Int. AR/Psep. 60—1, CERN, Geneva, Switzerland.

[49] M. M. Geiger, P. Lapostolle and B. Montague, La séparation des particules au moyen de champs hf, CERN, Report No. 61—26, CERN, Geneva, Switzerland.

[50] J. J. Murray, Mass Separation by Means of Microwave Linear Acceleration in Secondary Beams, Nucl. Instr. and Meth. 20, 26 (1963).

[51] W. K. H. Panofsky, W. A. Wenzel, Some Considerations Concerning the Transverse Deflection of Charged Particles in Radio-frequency fields, Rev. Sci. Instr. 27, 967 (1956).

[52] M. Yves Garault, Propriété générale d'un type d'onde sepapropageant dans le vide a la vitesse de la luniére et utilisable pur le déflexion de particules ultrarelativistes, Compt. rend. 254, 843 (1962).

[53] Louis deBroglie, Electromagnetic Waves in Waveguides and Cavities, Gauthiers-Villars, Paris, 1941.

[54] Davydov, Dorfman, Zalmanzon, Zeĭtlenok, Ekimov, Levin, Malyshev, Petelin, Petrunin, Popov, Trushin, Umanskiĭ, and Finkel'shteĭn, Deflecting System for Antiproton Channel at 5 GeV, Op. cit. [11].

[55] M. Yves Garault, Solutions coherentes de l'equation des ondes en coordonnees cylindriques valables quelle que la vitesse de phase, Compt. rend. 254, 1391 (1962).

[56] M. Yves Garault, Ondes electromagnetiques du type EH dans un guide cylindrique circulaire chargé par des iris métalliques, Compt. rend. 255, 2920 (1962).

[57] H. Hahn, Deflecting Mode in Circular Iris-loaded Wave Guides, Rev. Sci. Instr. 34, 1094 (1963).

[58] M. Bell, P. Bramham, B. W. Montague, Pulse-shortening in Electron Linear Accelerators and E″ Type Modes, Nature 198, 277 (1963).

[59] P. Bramham, R. F. Measurements on the First Metre of Electro-formed Loaded Waveguide for the Microwave Particle Separator, Op. cit. [11].

[60] O. A. Altenmuelle, R. R. Larsen, G. A. Loew, Investigations of Travelling-wave Separators for the Stanford Two-mile Linear Accelerator, Op. cit. [11].

[61] Bell, Bramham, Fortune, Keil, and Montague, RF particle separators, Op. cit. [11].

[62] Vagin, Veksler, Zubarev, Kuznetsov, Mukhin, Petukhov, Popov, Rubin, Semenyushkin, Stepanyuk, and Chekhlov, Electrodynamic Separation of Antiprotons with 5 GeV/c Momenta, Op. cit. [11]

[63] Vagin, Vysochanskiĭ, Mukhin, Rikhvitskiĭ, Semenyushkin, Stepanyuk, and Foltin, Experimental Investigations of Multiple Acceleration of Protons ($f = 69$ Mcs) in a 10 GeV Proton Synchrotron, Op. cit. [11]: Vagin, Panfilov, Semenyushkin, Stepanyuk, and Chekhlov, Some Results of Investigations of Multiple Acceleration of 69 Mcs in the Proton Synchrotron of the Joint Institute for Nuclear Research. Preprint, Joint Institute for Nuclear Research, 1406, Dubna, 1963.

[64] K. P. Myznikov, and I. N. Yalovoĭ, Extraction of Beam to a Target in a Proton Synchrotron by Excitation of Azimuthal Symmetry of the Magnetic Field, PTÉ No. 4, 19 (1963).

[65] E. Keil and W. W. Neale, A High Momentum Separated Particle Beam for Use with the 1.50 Metre British National Hydrogen Bubble Chamber at CERN, Op. cit. [11].

[66] E. Keil, Parameters for r.f. Separation of π and K at 100 GeV/c Design Momentum, CERN, AR/Int. PSep./62—3, 1962.

[67] E. Keil, Tolerances on r.f. Separator Parameters, CERN, AR/Int. PSep./63—3, 1963.

[68] B. W. Montague, The Application of Superconductivity to r.f. Particle Separators, CERN, AR/Int. PSep./63—1, 1963.

[69] P. B. Wilson, Investigation of the Q of a Superconducting Microwave Cavity. Nucl. Inst. and Meth. 20, 336 (1963).

[70] G. Goldhaber, S. Goldhaber, B. Peters, Separation of High-Energy Particles by Means of Strong Interactions, Nucl. Phys. 25, 502 (1961).

[71] Elektrofizicheskaya apparatura promyshlennogo izgotovleniya (Commercial Electrophysics Apparatus), Gosatomizdat, 1963.

Translated by J. G. Adashko